Faculty of Health, Science and Technology

Environmental and Energy Systems

Jesper Nyberg

Flow Distribution in Brazed Plate Heat Exchangers

A Parameter Study in COMSOL

Flödesfördelning i Hårdlödda Plattvärmeväxlare

En Parameterstudie i COMSOL

Master Thesis 30 ECTS credit points

Science Program in Environmental and Energy Engineering

June 2016

Supervisors: Wamei Lin & Kamal Rezk

Examiner: Roger Renström

Karlstad University 651 88 Karlstad Sweden
Tel +46 054-700 10 00 Fax +46 054-700 14 60
Information@kau.se www.kau.se

Abstract

Lubricants and liquid cooling are used in many industrial applications to ensure reliability and longevity of machinery. Oil cooling of both electrical and mechanical applications is of interest since oil is better suited for electrical applications than water and already available in the system as a lubricant. Brazed plate heat exchangers (BPHEs) have many advantages compared to other heat exchanger types commonly used in oil cooling applications. Flow maldistribution inside BPHEs can arise with highly viscous fluids like oil. Since flow is hard to measure when plate heat exchangers are brazed together, Computational Fluid Dynamics (CFD) can be used instead.

This study investigates parameters that could affect flow distribution inside BPHEs with the CFD-tool COMSOL Multiphysics. The study is made on three different geometries at different detail levels. The purpose of the study is to expand the knowledge about fluid behavior in BPHEs and how it affects efficiency. It was proved from the Bernoulli equation that flow velocity, gravity and Reynolds number were some parameters that could affect flow distribution inside BPHEs.

Two simplified models were built for evaluation of viscosity, gravity and Reynolds number. A more detailed model was provided by SWEP representing the fluid domain of a full-size distribution zone model. Model validation and mesh independence study were made with expressions due to the lack of experimental data. Investigations of viscosity, gravity and Reynolds number were made through isolation and alteration of the respective parameter. The validation and mesh independence study proved the models trustworthy and detailed enough to capture the physical behavior. Small deviations from expected validation results can be explained with the assumptions and simplifications made in the process.

Results show that flow maldistribution increases with viscosity differences between channels. Viscosity maldistribution is greater for oil than for water. It is important to consider how the fluid viscosity changes with temperature under the respective working conditions. Gravity has no effect on flow distribution as long as it acts along or opposite the main flow direction. As plate heat exchangers are generally placed vertically, gravity will not affect flow distribution. Gravity has a significant effect on flow distribution if plate packages are places horizontally. High Reynolds numbers have a positive effect on flow distribution and reduce the difference between highest and lowest velocities across the outlet. Very low flow velocities should therefore be avoided since it increases flow maldistribution.

Sammanfattning

Smörjmedel och vätskekylning används i många industriella applikationer för att garantera maskiners pålitlighet och livslängd. Oljekylning av både elektriska och mekaniska applikationer är intressant då olja är bättre lämpad för elektriska applikationer än vatten och redan finns tillgänglig som smörjmedel i systemet. Hårdlödda plattvärmeväxlare har många fördelar gentemot andra värmeväxlartyper som normalt används för oljekylning. Trots detta, kan felfördelning av flödet uppstå som resultat av höga viskositeter hos fluider som olja. Eftersom flödet är svårt att analysera när plattvärmeväxlare är lödda eller svetsade kan datorbaserade simuleringsverktyg användas som substitut till experimentella tester.

Den här studien undersöker parametrar som kan påverka flödesdistributionen inuti en hårdlödd plattvärmeväxlare med hjälp av simuleringsverktyget COMSOL Multiphysics. Studien genomförs på tre olika geometrier med olika detaljnivåer. Syftet med studien är att fördjupa kunskapen om flödet i hårdlödda plattvärmeväxlare och hur det påverkar effektiviteten. Det bevisades med Bernoullis ekvation att flödeshastighet, gravitation och Reynoldstal var några parametrar som avgör flödesfördelningen i hårdlödda plattvärmeväxlare.

Två förenklade modeller byggdes för utredningar av viskositet, gravitation och Reynoldstal. En mer detaljerad modell tillhandahölls av SWEP och representerade en fullstor distributionszons fluiddomän. Validering och känslighetsanalys av mesh gjordes med fysiska samband eftersom experimentella data saknades. Utredningar av viskositet, gravitation och Reynoldstal gjordes genom isolering och variering av respektive parameter. Valideringen och känslighetsanalysen visade att modellerna var pålitliga och detaljerade nog för att fånga det fysiska beteendet. De små avvikelserna från valideringsresultat kunde förklaras med de antaganden och förenklingar som gjordes i processen.

Resultaten visar att felfördelningen ökar med ökad viskositetsdifferens mellan kanalerna. Felfördelningen är större för olja än för vatten. Det är viktigt att ta hänsyn till hur viskositeten förändras med temperatur under de aktuella arbetsförhållandena. Gravitation har ingen effekt på flödesfördelningen så länge kraften verkar i samma eller i motstatt riktning som huvudflödet. Gravitation har däremot en betydande effekt om plattvärmeväxlaren placeras horisontellt. Höga Reynoldstal har en positiv effekt på flödesfördelningen och minskar differensen mellan de högsta och lägsta flödeshastigheterna över utloppet. För låga flödeshastigheter ska undvikas eftersom det ökar risken för felfördelning.

Preface

This is the last and examining work of the Master of Science in Energy and Environmental Technology at Karlstad University. The work is made in cooperation with SWEP International AB in Landskrona Sweden.

This work has been presented verbally in front of an audience familiar with the subject. The work has also been discussed at a special seminar where the author of this work has participated actively as an opponent to another master thesis work.

I would like thank my supervisors Wamei Lin and Kamal Rezk for the guidance and support necessary to get over the obstacles encountered during this work. I would also like to thank Christel Elmqvist Möller and Patrik Gerenmark at SWEP for the opportunity to visit the company and for a general discussion of the project. Last but not least, I want to thank Lars Nilsson for having persuaded me to carry out my thesis. It proved to be the right decision.

Table of Contents

Nomenclature

Latin Letters	Quantity	Unit
A	Area	m^2
C_p	Specific heat	kJ/kg·K
C	Constant	1
D	Diameter	m
f	Friction factor	1
F	External Force	N
g	Gravitation	m/s^2
h	Height	m
I	Wetted perimeter	m
k	Conductivity	S/m
l	Length to closest wall	m
L	Length	m
m	Mass	Kg
n	Normal vector	-
p	Pressure force	Pa
P	Pressure	Pa
q	Heat flux per area	W/m^2
Q	Heat flux	W
T	Temperature	°C, K
u	Velocity field	m/s
U	Velocity magnitude	m/s
V	Velocity	m/s
w	Width	m
x	x-coordinate	m
y	y-coordinate	m
z	z-coordinate	m
Re	Reynolds number	1

Greek Letters	Quantity	Unit
ε	Turbulent dissipation rate	m^2/s^3
α	Kinetic correction factor	1
ϱ	Density	kg/m^3
ν	Kinematic viscosity	m^2/s
σ	Constant	1
μ	Dynamic viscosity	Pa·s

Subscript/Superscript	Description
$( )_1$	Channel 1
$( )_2$	Channel 2
$\bar{}$	Mean value
$( )_h$	Hydraulic
$\dot{}$	Flow
Δ	Difference
$( )_p$	Potential
$( )_{cs}$	Cross-sectional

∇	Gradient
$(\ )^T$	Transpose
$(\ )_T$	Turbulent
$(\ )_k$	Turbulent kinetic energy
$(\ )_\varepsilon$	Turbulent dissipation rate
$(\ )_w$	wall/closest wall
$(\hat{\ })$	Maximum possible value
$\rightarrow$	Vector/Vector field
$(\ )_0$	Initial defined value
$(\ )_{inlet}$	Inlet
$(\ )_{cold}$	Cold channel
$(\ )_{hot}$	Hot channel

Abbreviations	
BPHE	Brazed Plate Heat Exchanger
CFD	Computational Fluid Dynamics
PDE	Partial Differential Equation
PHE	Plate Heat Exchanger
FVM	Finite Volume Method
FEM	Finite Element Method

1 Introduction

1.1 Background

Lubricants are used in many industrial applications to ensure reliability and longevity of machinery (Rangaprasad & Gupta 2015). Proper lubrication prevents wear and heat generation by minimizing friction between moving parts (Rangaprasad & Gupta 2015). Lubricants also have a cooling effect as they flow over surfaces where heat is generated, thus carrying heat away (Rangaprasad & Gupta 2015). The most common form of lubricant is the oil used in combustion engines for automotive applications (Rangaprasad & Gupta 2015). Lubricants also play a vital role in power sources that have been developed to replace combustion engines. Fuel cells are one of the most promising technologies to replace combustion engines and manage the increased environmental requirements (Wang et al. 2015). Electrical motors are a vital part of today's fuel cell technology. The compactness of these motors leads to a problem where air cooling may not be sufficient due to low convective heat transfer coefficients (Davin et al. 2015). Cooling is, as well as lubrication, essential to ensure engine reliability and functionality (Bonnett 2001). The properties of water make it inappropriate for cooling of electrical applications due to devastating leakage effects. Oil is already available as a lubricant in many industrial applications including both combustion engines and electrical motors. Unlike water, oil lubricates the system, prevents corrosion and does not conduct electricity. These properties make oil suitable for both electric and pure mechanical applications. Regardless if oil is used for lubrication or cooling, it will be heated and require cooling to regain its properties. Despite the many advantages of oil and its properties, there are few studies made about oil cooling (Davin et al. 2015).

Cooling is accomplished through allowing two flows at different temperatures to meet and exchange energy in a heat exchanger device. Various heat exchangers have been developed over the years, each with their respective advantages and disadvantages. Shell-and-Tube Heat Exchangers, known for their customizability, are commonly used in oil cooling applications (Shah & Sekulic 2003). However, there are many advantages of brazed plate heat exchangers (BPHEs) that could make them better suited for oil cooling applications. A BPHE is a compact plate heat exchanger, which means that the heat transfer surface is large per unit volume (Shah & Sekulic 2003). The required surface area of a plate heat exchanger is down to one-third of the area needed in a shell-and-tube heat exchanger for the same operating conditions (Shah & Sekulic 2003). This reduces the cost, weight, internal and external volume of the heat exchanger (Shah & Sekulic 2003). Brazed plate heat exchangers also lack the vibrations, thermal stresses, and noise that characterize shell-and-tube exchangers (Shah & Sekulic 2003). Even though the advantages of using a BPHE instead of a shell-and-tube are numerous, a problem arises with highly viscous fluids like oil. High viscosities can lead to flow maldistribution within the BPHE (Shah & Sekulic 2003). This is particularly interesting in cooling applications since viscosity increases with decreasing temperature (Shah & Sekulic 2003).

Few flaws and many benefits make plate heat exchangers (PHE) one of the most common heat exchanger types. The extensive usage has created a need for efficient and reliable design to optimize system performance (Aslam Bhutta et al. 2012). The most reliable approach to analyze thermal and hydraulic performance is to conduct experiments and measure interesting quantities. It has been proved that Computational Fluid Dynamics

(CFD) can be a useful substitute to experimental trials, especially in the development of plate heat exchangers (Gullapalli & Sundén 2014). This is particularly true when interesting quantities are difficult to measure or when the geometry does not allow it. Flow distribution is a typical example of a quantity that is difficult to measure if the plate heat exchanger is welded or brazed together (Sarraf et al. 2015). To fully use the potential of BPHEs, it is important that fluids distribute evenly over the available heat transfer surfaces. This is a case where there is much work to be saved by the use of CFD.

The majority of plate heat exchanger studies already made with CFD have used the software ANSYS. Studies with flow phenomenon as one of many results have been done in ANSYS by Freund & Kabelac (2010), Jeong et al. (2009), Gullapalli (2011), Gullapalli & Sundén (2014), Han et al. (2010), Galeazzo et al. (2006), Lee & Lee (2014), Lee & Lee (2015) and Tsai et al. (2009). Sarraf et al. (2015) evaluated flow characteristics in STAR CCM+. Water is used in most of these studies due to its availability and simplicity. As described above, a lot of applications rely on oil or other highly viscous fluids with different properties than water. Moreover, not many studies focus on flow distribution despite its importance to plate heat exchanger efficiency.

1.2 Aim

This study aims to examine parameters that are believed to affect flow distribution in plate heat exchangers. The purpose of the study is to expand the knowledge of how fluid properties and working conditions affect plate heat exchanger efficiency. The study is made with respect to oil cooling and water applications and aims to answer following questions:

- What parameters affect flow distribution in plate heat exchangers?
- How does the parameters affect flow distribution and under what conditions?
- What can be done to avoid flow maldistribution due to the respective parameter?

2 Theory

2.1 Fluid Theory

The Bernoulli equation is applicable along a streamline in steady and incompressible flow and relates flow energy between two points. It is originally formed as an energy balance but can also be expressed in terms of pressure (Pa) or head (m). It states that the sum of flow, kinetic and potential energy is constant along a streamline where friction and compressibility can be neglected. The Bernoulli equation is a powerful tool but also based on assumed conditions that seldom occur in real applications. The application of the Bernoulli equation assumes steady and incompressible flow with negligible viscous effects. The equation is also based on negligible heat transfer and work within the system. It should be remembered that the Bernoulli equation is developed for flow along a streamline. (Cengel & Cimbala 2010)

Flow from point 1 to point 2 is considered along a streamline in Figure 1. The pipe is vertically placed, circular, of length L and diameter D. The pressure between these two points can be related to each other through the Bernoulli equation in pressure form (1). Since point 2 is defined at zero height, the height difference between the two points is z_1. Static pressure (P) in both point 1 and 2 equals the atmospheric pressure and the kinetic correction factor (α) is the same in both points as the flow regime is the same. The friction factor (f) (2) for circular channels is defined as a constant divided by the Reynolds number evaluated at the mean velocity ($\overline{V}$), density ($\overline{\rho}$) and viscosity ($\overline{\mu}$). The Bernoulli equation can be simplified (3) when the friction factor expression (2) is included. Mean velocity is defined as half of the sum of the inlet (V_1) and outlet velocity (V_2) of the studied channel (4). Combining Eq. 3 and 4, and a rearrangement of terms leave an expression that relates velocities between the two points (5).

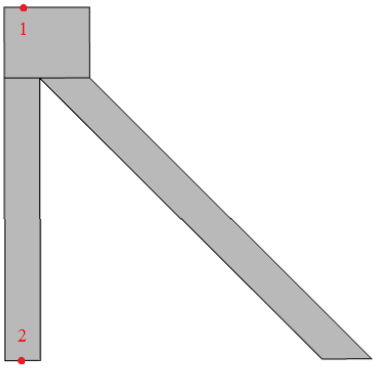

Figure 1. Pressure at two points along a streamline can be related through the Bernoulli equation.

$$P_1 + \alpha_1 \frac{\rho \cdot V_1^2}{2} + \rho_1 \cdot g \cdot z_1 = P_2 + \alpha_2 \frac{\rho \cdot V_2^2}{2} + \rho_2 \cdot g \cdot z_2 + f \frac{L}{D_h} \frac{\overline{\rho}\overline{V}^2}{2} \quad (1)$$

$$f = \frac{64}{\mathrm{Re}} = \frac{64 \cdot \overline{\mu}}{\overline{\rho} \cdot \overline{V} \cdot D_h} \quad (2)$$

$$\frac{V_1^2}{2} + g \cdot z_1 = \frac{V_2^2}{2} + \frac{32 \cdot L \cdot \bar{\mu} \cdot \bar{V}}{\bar{\rho} \cdot D_h} \tag{3}$$

$$\bar{V} = \frac{V_1 + V_2}{2} \tag{4}$$

$$\frac{V_2^2}{2} + \frac{16 \cdot L \cdot \bar{\nu} \cdot V_2}{D_h} = \frac{V_1^2}{2} + g \cdot z_1 - \frac{16 \cdot L \cdot \bar{\nu} \cdot V_1}{D_h} \tag{5}$$

$$V_2 = f(V_1, g, z, \nu, L, D_h) \tag{6}$$

$$\dot{m}_2 = f(V_1, \rho, g, z, \nu, L, D_h) \tag{7}$$

From the resultant expression (5) it can be seen that the outlet velocity (V_2) depends on the inlet velocity (V_1), gravity (g), height difference (z), kinematic viscosity (ν), length (L) and hydraulic diameter (D_h) of the studied channel (6). If the outlet areas are the same in a system of several, the velocity at each outlet is decisive for the mass flow over that boundary (7). This means that a change in each of the parameters above can be of great importance when studying flow distribution inside system with several flow channels.

This study focuses on the effects of viscosity, gravity and Reynolds number on flow distribution. Since flow velocity throughout the domain is crucial for flow distribution, it was also a natural choice for the investigations. Viscosity was chosen since it is the only parameter in the expression above (6) relating flow velocity to fluid properties. Also, viscosity was discussed as one parameter of industrial interest in a meeting with SWEP (Gerenmark 2016). Gravity was also discussed at this meeting and therefore included in the investigations. The chosen parameters are briefly presented below.

2.1.1 Viscosity

Viscosity is a property used for describing fluid resistance to flow. Fluid flow involves fluid layers sliding over each other and viscosity defines the frictional force between these layers. A higher frictional force leads to higher viscosity, as in the case of oil compared to water. Viscosity is both pressure and temperature dependent, but pressure effects are often neglected. For liquids, the viscosity decreases with increasing temperature since the higher energy content help the molecules to overcome collision forces. (Cengel & Cimbala 2010)

2.1.2 Gravity

Gravity can be defined as a force acting on a mass in the downwards direction (Cengel & Cimbala 2010). The magnitude of the force is proportional the object mass (m) and the gravitational constant (g) (8). When a force acts along a path it is converted into energy. As fluid flow inside plate heat exchangers occur along paths during constant impact of gravity, it is interesting to evaluate whether gravity affects flow distribution or not. It gets interesting as the most common orientation of the plates involve vertical flow both in the downwards and upwards direction. According to the Bernoulli equation (1), a height difference leads to an increase in potential pressure equal to the product between the density (ρ), gravitational constant (g) and height (h)(9).

$$F = m \cdot g \tag{8}$$

$$\Delta P_p = \rho \cdot g \cdot z \tag{9}$$

2.1.3 Reynolds Number/Velocity

Since the flow distribution is dependent of velocity (6), it is also dependent of Reynolds number. A higher velocity gives a higher Reynolds number. Flow is either laminar or turbulent depending on the flow conditions. Reynolds number has been developed as a criterion to determine whether flow in a studied domain is laminar or turbulent. It describes the relation between inertial forces, in terms of density (ρ), average velocity ($\overline{V}$) and hydraulic diameter (D_h), to viscous forces in terms of dynamic viscosity (μ) (10). Internal flow is said to be laminar if the Reynolds number is less than 2300, transitional between 2300 and 4000, and turbulent if higher than 4000. (Cengel & Cimbala 2010)

$$\mathrm{Re} = \frac{\rho \cdot \overline{V} \cdot D_h}{\mu} \tag{10}$$

Due to the complex geometries of the flow channels, Reynolds number in plate heat exchangers is often defined differently than for rectangular ducts. A cross section of a plate heat exchanger flow channel may look like in Figure 2, depending on where the cut is positioned. The colored area in Figure 2, between the sine shaped curves, represents the fluid domain with a main flow direction normal to the cut. The Reynolds number for a channel of this shape is calculated in the same way as above (10) but with another definition of the hydraulic diameter (D_h) (11). The hydraulic diameter for a rectangular duct depends on the cross-sectional area (A_{cs}) and the wetted perimeter (I) (11) (Cengel & Cimbala 2010). Since the channel height is insignificant in comparison to the total width in Figure 2, it can be neglected from the expression denominator. If the height is deleted from the denominator and the expression is simplified further, the hydraulic diameter can be expressed as a function of height only (12). The Reynolds number can be calculated using this hydraulic diameter instead (13). Since there are typically large velocity gradients inside plate heat exchangers, a better way of expressing Reynolds number would be with the mass flow through the domain. A multiplication by a dimensionless width ratio gives a Reynolds number expression containing mass flow (14). This is a definition that SWEP use for calculating Reynolds number inside BPHEs. Both Reynolds number definitions will be used in this study, according to Eq. 10 and 14.

$$D_h = \frac{4 \cdot A_{cs}}{I} = \frac{4 \cdot w \cdot h}{2w + 2h}, \qquad (w >> h) \tag{11}$$

$$D_h = 2h \tag{12}$$

$$\mathrm{Re} = \frac{\rho \cdot \overline{V} \cdot 2h}{\mu} \tag{13}$$

$$\mathrm{Re} = \frac{\rho \cdot \overline{V} \cdot 2h}{\mu} \cdot \frac{w}{w} = \frac{\dot{m} \cdot 2}{\mu \cdot w} \tag{14}$$

Figure 2. A cross section of a plate heat exchanger is complex and another definition of Reynolds number is required. The colored area represents the fluid domain.

2.1.4 Shell Rimula 40

Shell Rimula 40 is an engine oil commonly used in industrial applications (Gerenmark 2016). The investigations in this study were made with water and Shell Rimula 40 as working fluids. Shell Rimula 40 properties needed for investigations were retrieved from the internally used calculation software *SSP G7* at SWEP. (SWEP International AB 2015)

2.2 Heat Exchangers

A heat exchanger is a unit that allows two mediums at different temperatures to exchange thermal energy. Heat exchangers can be used for heat transfer between both solids and liquids. The most common use of heat exchangers involves heating, cooling, evaporation or condensation of fluids. In the industry, the aim of heat exchanger usage could be to recover or reject heat, sterilize, pasteurize, fractionate, distill, concentrate, crystallize or thermally control a process fluid. They are directly used in process, power, petroleum, transportation, air-conditioning, refrigeration, cryogenic, heat recovery, alternative fuel, and manufacturing industries but also occur as vital parts of different products. (Shah & Sekulic 2003)

Two major ways to classify heat exchangers are by surface compactness or construction. These classifications are clarified in Figure 3, where β represents heat transfer area to total volume. A liquid to liquid heat exchanger is considered compact when the heat transfer area exceeds 400 m^2/m^3 and non-compact for less. Another distinction is made between construction types as visible in Figure 3. Two common heat exchangers are the shell-and-tube and plate heat exchanger. These belong to the tubular and plate-type constructions respectively. Plate heat exchangers are further considered compact unlike shell-and-tube heat exchangers. (Shah & Sekulic 2003)

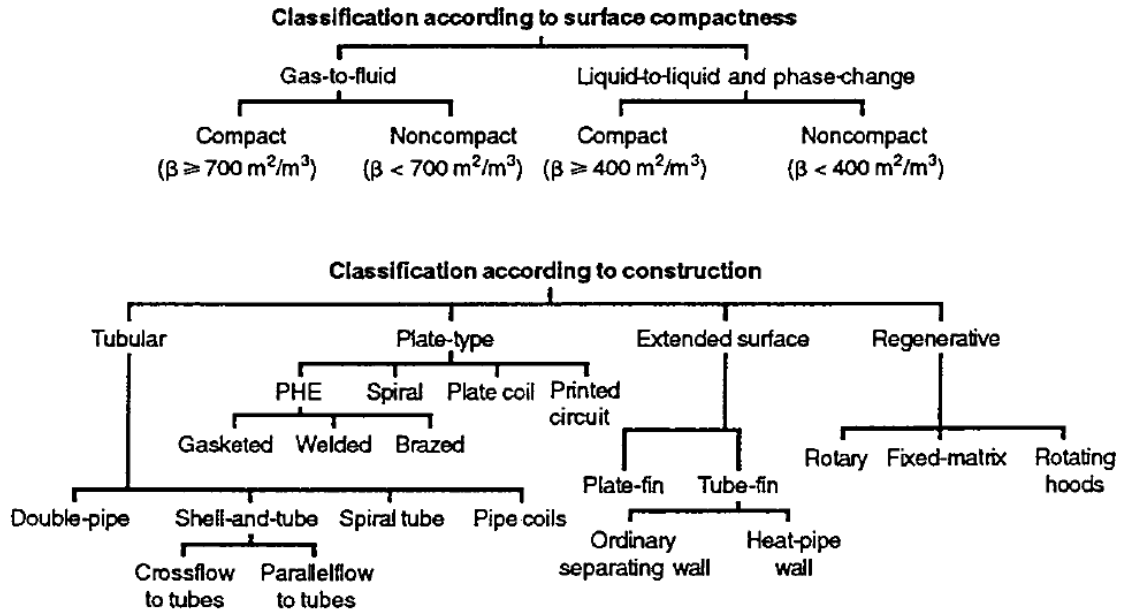

Figure 3. Classifications of heat exchangers can be based on surface compactness or construction types. (Shah & Sekulic 2003)

2.3 Brazed Plate Heat Exchangers

As mentioned in the previous section, plate heat exchangers belong to the group of compact heat exchangers, which means that the heat transfer surface is large per unit volume. This makes it possible to reduce the required size, weight, cost and internal volume in contrast to the widely used shell-and-tube exchanger. Plate heat exchangers consist of a number of thin stainless steel or titanium plates. The plates are usually cold worked into repetitive patterns. The plates are stacked together where the number of plates depends on the working conditions. Resulting plate packages are generally placed vertically as in Figure 4. Different patterns have been developed, but a common one is the chevron or herringbone pattern visible in Figure 4. The angle of the chevron pattern varies for different applications. Every other plate is rotated 180 degrees during assembly. The crossing patterns yield many contact points to provide stability. Fluid flow occurs in the complex flow channels created in the space between the plates. The tortuosity and interruptive geometry of the channels lead to turbulence which increases heat transfer and pressure drop. The complexity of the channels makes them inappropriate for viscous flow or fluids containing solid particles. (Shah & Sekulic 2003)

Ports are placed at each of the four corners of the plates, two inlets and two outlets. As the plates are stacked, the ports create a distribution header at each corner of the plate package were the fluids enter the fluid channels. From each of the inlets, there is only access to every other fluid channel due to gaskets, welding or brazing. It is possible to change flow arrangement through different port placements. First, a difference is made between a single-pass or multi-pass unit. This indicates the number of times a flow is allowed to pass a heat transfer surface within the plate heat exchanger. The difference between a single-pass and multi-pass unit is clarified in Figure 5. The majority of plate heat exchangers are single-pass units. Secondly, internal flows can occur differently relative each other. Counter flow is the most common where fluids flow along the same path but in direct opposite directions. (Shah & Sekulic 2003)

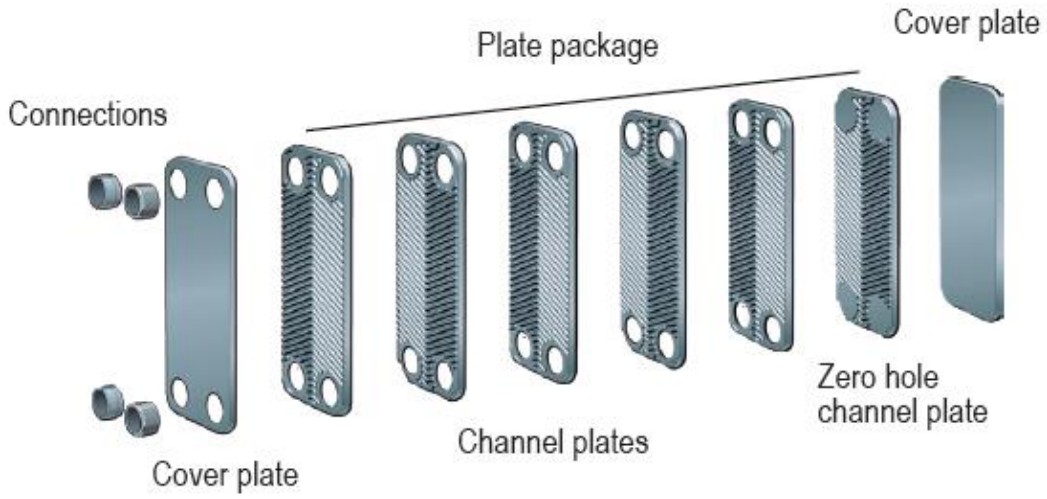

Figure 4. A plate heat exchanger consists of cover plate, plate package and connections mounted together as illustrated by SWEP International AB (2015b).

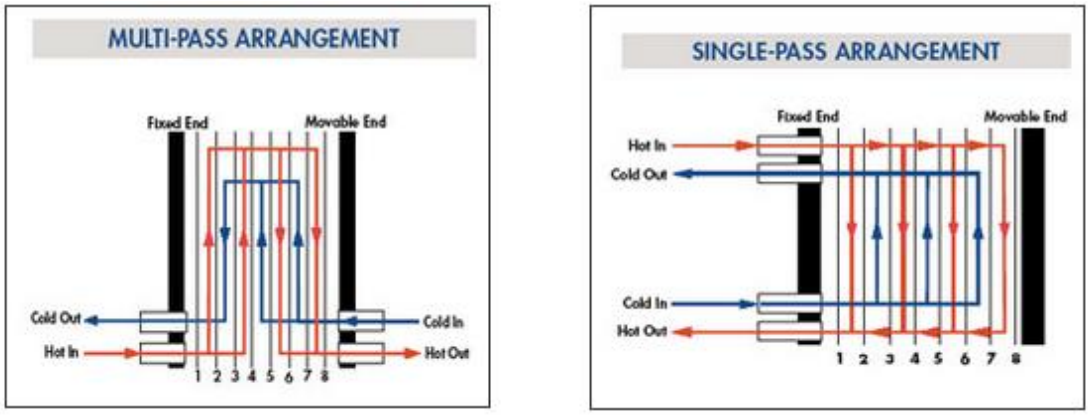

Figure 5. Examples of multi-pass and single-pass arrangements inside plate heat exchangers as illustrated by Baode Heat Exchanger Co. (2009).

Plate heat exchangers are classified in three groups depending on how the plates are joined together. Plate heat exchangers are gasketed, welded or brazed, each with respective advantages and disadvantages. The working principle of these types is the same**.** Brazed plate heat exchangers have evolved through limitations of gasketed plate heat exchangers. The gaskets are weak points because of their sensitivity to aggressive fluids, high pressures and temperatures. When plate heat exchangers are brazed, there is no need for gaskets or the external frame of gasketed plate heat exchangers. Therefore, BPHEs are smaller than gasketed plate heat exchangers. Also, the brazings allow higher operating pressures and temperatures, but at the same time prevent disassembly of the unit. The brazing is done with copper, but other brazing materials could be used if the applications involve aggressive fluids. (Shah & Sekulic 2003)

2.3.1 Studies on Plate Heat Exchangers

The increasing requirement of performance and efficiency makes the development of new plate types to a vital part of the industry (Gullapalli & Sundén 2014). Gullapalli & Sundén (2014) explained that design and development are mainly about increasing thermal performance by variation of interesting parameters. A lot of empirical correlations exist that relate geometrical parameters to thermal performance, but these correlations tend to lack generality (Gullapalli 2011). In recent years, CFD have been proved to be useful in the development of plate heat exchangers (Gullapalli & Sundén 2014). The interest in plate heat exchangers and the availability of both numerical and empirical methods have led to a high number of studies made on this particular area.

Gullapalli & Sundén (2011) created a generally applicable method by using enthalpies and pressures. The method was thought as implementable in calculation or simulation software without convergence problems (Gullapalli & Sundén 2011). A discretization of the computational domain led to a possibility to calculate heat transfer coefficients and pressure drops by iterative methods (Gullapalli & Sundén 2011). Dović et al. (2009) developed a generalized correlation to describe thermal and hydraulic performance in terms of Nusselt number and friction factor for single-phase flow in a plate heat exchanger. From observations, correlations were developed for chevron angles between 15 and 65° and for chevron height to pitch ratios between 0.26 and 0.4 (Dović et al. 2009). Both these studies were of experimental character and resulted in good agreement with validation data.

Studies have also been made with CFD-tools. The majority of the studies use the common CFD-tool ANSYS. Han et al. (2010) analyzed temperature, pressure and flow fields numerically and compared the results to experimental data. The CFD-model was based on an available prototype and its operational conditions (Han et al. 2010). Gullapalli & Sundén (2014) studied heat transfer and pressure drop to investigate the performance dependency of design and the possibility to use CFD in the design process. Simulations were run on sections of, as well as complete, flow channels (Gullapalli & Sundén 2014). Gullapalli (2011) also evaluated the important parameters when ANSYS was used for design and development. The effect of mesh, turbulence model and simulation methods on heat transfer and pressure drop was evaluated (Gullapalli 2011). The results showed that CFD-tools were in need of universally applicable turbulence models and boundary conditions (Gullapalli 2011).

Galeazzo et al. (2006) used a CFD-model to simulate flow and heat transfer in a four channel plate heat exchanger with smooth plates. Both parallel and series connections were investigated in one and three dimensions (Galeazzo et al. 2006). Lee & Lee (2014) made a detailed study of flow with large eddy simulation (LES). Different geometrical parameters influence on the friction and Colburn factor were investigated together with heat transfer and pressure drop (Lee & Lee 2014). A representative part of the plate heat exchanger was modeled in ANSYS (Lee & Lee 2014). In another study by Lee & Lee (2015), focus was to investigate friction and Colburn factor as a function of chevron angle, pitch and height. This study was also made on a representative part of the plate heat exchanger (Lee & Lee 2015).

Jeong et al. (2009) evaluated pressure drop and heat transfer in plate heat exchangers with three different plate patterns. Numerical results were compared to experimental ones for validation (Jeong et al. 2009). Freund & Kabelac (2010) performed an experimental and

numerical study of local heat transfer coefficients. The study results varied with turbulence model (Freund & Kabelac 2010). Tsai et al. (2009) modeled a plate heat exchanger consisting of two flow channels. The model represented the complete flow channels, including inlet and outlet as well as the plate patterns (Tsai et al. 2009). Focus was on investigating pressure drop and flow distribution that was later compared to experimental results (Tsai et al. 2009).

Sarraf et al. (2015) used STAR CCM+ instead of ANSYS to evaluate the relation between flow structure and friction coefficient. Experimental results were used for validation of thermal and hydraulic performance. Both laminar and turbulent cases were analyzed. (Sarraf et al. 2015)

2.4 Computational Fluid Dynamics

Experimental analyzes can be hard under certain conditions. In plate heat exchangers a situation like this occur when flow is to be analyzed in a welded or BPHE (Sarraf et al. 2015). Therefore, computer based simulations of heat transfer, fluid flow, chemical reactions etc. have been developed as a tool for detailed analyzes of complex systems (Versteeg & Malalasekera 2007). Tools of this type are called Computational Fluid Dynamics or CFD (Versteeg & Malalasekera 2007).

Research and development of aircraft and space shuttles have been using CFD for flow analysis since the 1960s. Since then, a lot of other applications have relied on CFD to predict system behavior. The nature of fluid flow is complex and work based on flow equations is therefore complicated and time-consuming. The recent increase in computer performance has created great interest in CFD, which has been frequently implemented in different industries since the 1990s. Many have also discovered the benefits of simulations as a substitute to experimental tests. Simulations are generally less time-consuming than experiments even if some simulations can take days to complete. As already mentioned above, some systems may be hard or dangerous to analyze experimentally but very easily analyzed with CFD. The detail level of results in CFD is hard to achieve with experiments, even under controlled conditions. Costs of CFD are mainly due to licenses that are bought on an annual basis or even less frequently. The total costs are usually low in comparison with a precise experimental setup. (Versteeg & Malalasekera 2007)

Today's available CFD-tools are numerous but the basic function is the same. All codes refer to numerical algorithms that calculate physical behavior. The function of a CFD-tool is divided into three main parts, pre-processing, solver, and post-processing. (Versteeg & Malalasekera 2007)

2.4.1 Finite Volume & Finite Element Method Solvers

The physical behavior of a system can be described with partial differential equations (PDEs), i.e. differential equations depending on two or more variables. Since PDEs are hard to solve analytically, a discretization is required to express these in numerical terms implementable in a computer. A solution to these numerical approximations is an approximate solution to the partial differential equations, since the PDEs are approximated with discrete equivalents (COMSOL Inc. 2016c). Two commonly used methods for these approximations are the Finite Volume (FVM) and the Finite Element Method (FEM) (Autodesk Inc. 2015).

A FVM solver calculates the state of each defined control volume using conservation laws (CFD Online 2012). The first step of the FVM is the division of the computational domain into control volumes (CFD Online 2012). Interesting variables are evaluated at a center node of these control volumes (CFD Online 2012). An integration of the governing partial differential equations is made over the control volumes defined in the pre-processing tool (Versteeg & Malalasekera 2007). Interpolation is needed to describe the fluxes between nodes since the continuity is eliminated (CFD Online 2012). The resultant discretized equations describe the conservation of properties inside each control volume (CFD Online 2012). A solution to these equations is calculated by a computer using iterative methods. Two of the most used solver methods are the SIMPLE (Semi-Implicit Method for Pressure Linked Equations) and the TDMA (Tri-Diagonal Matrix Algorithm) (Versteeg & Malalasekera 2007).

The first step of a FEM solver is the so called weak formulation. In the weak form, the equation is no longer required to yield an absolute result. This formulation is commonly done with the Galerkin method of weighted residuals. The governing PDEs are multiplied with a space function that is assumed to belong to a so called infinite-dimensional Hilbert space and to have properties comparable to a common vector space. The resultant equation is integrated by parts to yield the weak formulation of the partial differential equation. In this way, the solution to the PDEs is expressed in terms of this space-function rather than in absolute values. The weak formulation and the Galerkin method is one possible way to transform analytical expressions into numerical approximations. (COMSOL Inc. 2016c)

The domain is later divided into elements with nodes along the borders (Logan 2007). Discretization makes it possible to search for an approximate solution to the infinite-dimensional Hilbert space in a finite-dimensional subspace. This is done through definition of a basis function and coefficient for each node. Basis functions and coefficients are set up as linear combinations to approximate the infinite solution in the finite subspace, where the coefficients are the unknowns. Every weak formulation is discretized once for every space function. The discretized version of the weak formulation thereafter creates a system of equations where the dimension depends on the number of space functions in the weak formulation. The solution to this system of equations can then be calculated through vector algebra. According to these steps the solution will only represent an approximation of the real solution. (COMSOL Inc. 2016c)

2.5 COMSOL Multiphysics

COMSOL Multiphysics is a CFD-software based on FEM (COMSOL Inc. 2016a). The finite element method makes COMSOL handle complex geometries easier than software based on the finite volume method (CFD Online 2011; CFD Online 2012).

The term *Multiphysics* refer to the simulation of several simultaneous physical phenomena such as fluid flow, heat transfer or chemical reactions that may depend on each other. At startup, the user defines the study dimension, physics involved, and if the study is time-dependent or stationary. The whole pre-process is done using the model builder where nodes represent the necessary steps before the numerical calculations can be done. The geometry node is used for building or importing geometries, and domain materials are defined including their properties using the materials node. Included physics can be found as separate nodes under which the respective boundary conditions are defined. Mesh is built manually or automatically using the mesh node. After meshing, the solvers calculate

the physical behavior of the system with respect to the boundary conditions. Study results are saved and can be analyzed under the results node. (COMSOL AB 2015)

2.5.1 Governing Equations & Boundary Conditions

Numerical solvers have to converge in order to find a solution to a problem defined by its equations. In COMSOL, these equations are defined through the choice of physics and boundary conditions. The choice of physics leads to a definition of governing equations solved by the solver to calculate system behavior. Each boundary condition is associated with one or several equations that apply where the boundary condition is defined. These equations determine how the solver treats the boundaries and thereby also the convergence of the solution. The most important governing equations and boundary conditions for this study are briefly explained in this section.

Heat transfer in fluids is defined over the fluid domain to account for the heat transfer and temperature change within the domain. The conservation of energy is calculated through relating temperature change with time, convection, conduction, and heat sources to each other (15). In stationary problems, the temperature change with time is zero and the first term cancels out. The heat conduction is calculated with the conductivity and temperature gradient (16). (COMSOL AB 2015)

$$\rho C_p \frac{\partial T}{\partial t} + \rho C_p \vec{u} \cdot \nabla T + \nabla \cdot \vec{q} = Q \tag{15}$$

$$\vec{q} = -k \nabla T \tag{16}$$

Fluid properties are defined on the fluid domain to account for the fluid behavior. Laminar fluid flow is calculated with the Navier-Stokes equations for conservation of momentum (17) and mass (18). The left side of the momentum equation describes inertial forces. These are related to the pressure forces (p), viscous forces (μ) and external forces (F) on the right. External forces (F) are *volume forces*, defined in the node as specific weight in vector form. The mass conservation principle is met through the simultaneously solved continuity equation (18). (COMSOL AB 2015)

$$\rho\left(\vec{u} \cdot \nabla\right)\vec{u} = \nabla \cdot \left[-pI + \mu\left(\nabla \vec{u} + \left(\nabla \vec{u}\right)^T\right)\right] + \vec{F} \tag{17}$$

$$\rho \nabla \cdot \left(\vec{u}\right) = 0 \tag{18}$$

When turbulence occurs, ordinary Navier-Stokes equations require fine mesh and in turn high computational capacity to capture flow details. Instead Reynolds-averaged Navier-Stokes equations (RANS) can be used to account for added behavior in turbulent flow. This model simplifies calculations through dividing flow behavior into mean values and fluctuations. Turbulence effects are modeled with a specified turbulence model and integrated into these equations. This makes it possible to avoid resolving every little flow detail. There are several ways of modeling turbulence and they have their respective advantages and disadvantages. The *low Reynolds number k-ε* model was used in this study. (COMSOL AB 2015)

The momentum equation (17) is extended with the eddy or turbulent viscosity (μ_T) for turbulent flow (19). The momentum equation is still solved together with the mass conservation principle (18). The low Reynolds number k-ε model solves for the turbulent kinetic energy (k) (20) and the turbulent dissipation rate (ε) (21). These expressions are dependent of viscosity (μ), density (ρ), velocity (u), eddy viscosity (μ_T), a production term (P_k), distance to the closest wall (l_w) and empirical constants (σ_k, σ_ε, $C_{\varepsilon 1}$, $C_{\varepsilon 2}$). (COMSOL AB 2015)

$$\rho\left(\vec{u}\cdot\nabla\right)\vec{u} = \nabla\cdot\left[-pI + \left(\mu+\mu_T\right)\left(\nabla\vec{u}+\left(\nabla\vec{u}\right)^T\right)\right] + \vec{F} \tag{19}$$

$$\rho\left(\vec{u}\cdot\nabla\right)k = \nabla\cdot\left[\left(\mu+\frac{\mu_T}{\sigma_k}\right)\nabla k\right] + P_k - \rho\varepsilon \tag{20}$$

$$\rho\left(\vec{u}\cdot\nabla\right)\varepsilon = \nabla\cdot\left[\left(\mu+\frac{\mu_T}{\sigma_\varepsilon}\right)\nabla\varepsilon\right] + C_{\varepsilon 1}\frac{\varepsilon}{k}P_k - C_{\varepsilon 2}\rho\frac{\varepsilon^2}{k}f_\varepsilon\left(\rho,\mu,k,\varepsilon,l_w\right) \tag{21}$$

A starting temperature can be used as an *initial value* for the solver. Boundaries where no heat transfer is defined are defined as *thermally insulated* by default. This boundary condition states that the conductive heat transport over a boundary is zero (22). *Thermal insulation* sets the temperature difference across that boundary to zero, which in turn leads to no heat flux. If a *Heat Flux* is defined over a boundary, a positive heat flux means a contribution of energy to the system (23). The heat flux can be defined as a general inward heat flux, convective heat flux or an overall heat transfer rate. (COMSOL AB 2015)

$$-\vec{n}\cdot\vec{q} = 0 \tag{22}$$

$$-\vec{n}\cdot\vec{q} = q_0 \tag{23}$$

A definition of the *temperature* is needed somewhere in the domain, typically at the inlet that is responsible for an inward energy flux (24). Using the *Outflow* boundary condition, it is possible to define the boundaries where energy outflow occur. The equation states that the heat transfer over a boundary is by convection only, due to a temperature gradient equal to zero (25). (COMSOL AB 2015)

$$T = T_0 \tag{24}$$

$$-\vec{n}\cdot\vec{q} = 0 \tag{25}$$

Fluid flow along or near walls is defined through the boundary condition *wall*. There are several ways of defining near wall behavior in COMSOL. The *wall* condition can be defined as *no slip, slip, sliding wall, moving wall, leaking wall,* or *slip velocity*. For turbulent flow using the low Reynolds number k-ε model, the *no-slip*, *sliding wall* and *moving wall* are available as versions with *wall functions*. The no-slip condition sets the fluid velocity at the wall to zero and a boundary layer is built up in the direction normal to the surface (26). The no-slip condition was used throughout this study. (COMSOL AB 2015)

$$\vec{u} = 0 \tag{26}$$

Inlet is defined at a boundary where mass is entering the system. The inflow velocity to the domain is defined as a velocity or velocity field in the direction negative to the outward normal of the boundary (27). At boundaries where mass is leaving the domain, the *outlet* boundary condition is defined. The outlet condition can be defined as a pressure, velocity or laminar outflow. When defined as pressure, the normal stress over the boundary is equal to the defined pressure (28), (29). (COMSOL AB 2015)

$$\vec{u} = -U_0 \cdot \vec{n} \tag{27}$$

$$\left[-pI + \mu\left(\nabla\vec{u} + \left(\nabla\vec{u} \right)^T \right) \right]\vec{n} = -\hat{p}_0 \vec{n} \tag{28}$$

$$\hat{p}_0 \leq p_0 \tag{29}$$

2.6 SWEP

SWEP was founded in 1983 and has grown into one of the world's largest supplier of BPHE technology. Applications include district heating, air conditioning, process industry, and marine technologies among others. The company has been a part of the Dover Corporation since 1994. The head office is located in the Swedish city of Landskrona, but the company is represented in 50 different countries over the world. (SWEP International AB 2015a)

3 Method

3.1 Building Simplified Models

The flow geometry inside plate heat exchangers is complex due to the crossing herringbone patterns. Simulations of complete flow channels, from inlet to outlet in Figure 6, require high performance computational power and long computational times. When available hardware is not enough, simplified models can be used instead to evaluate flow distribution. Two simplified models were used for the investigation of parameters in this study. These investigations were later implemented in a full-size model representing the distribution zone in Figure 6. This model can be seen in Figure 7 and represents the distribution zone of one channel fluid domain.

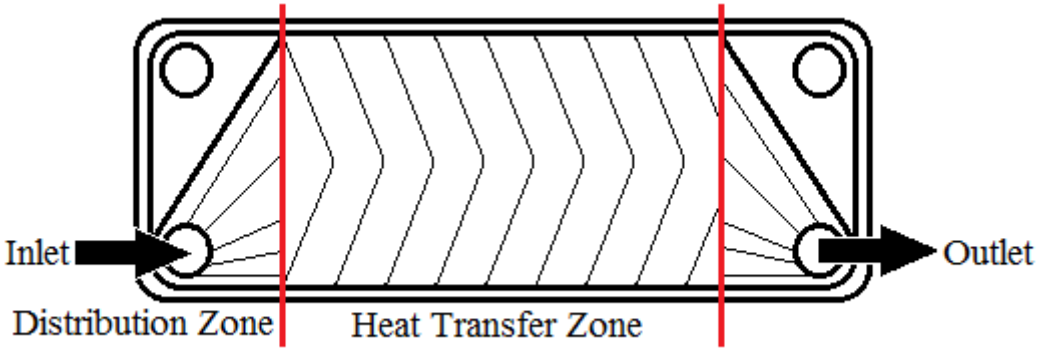

Figure 6. A plate heat exchanger fluid channel can be divided into a distribution zone and a heat transfer zone.

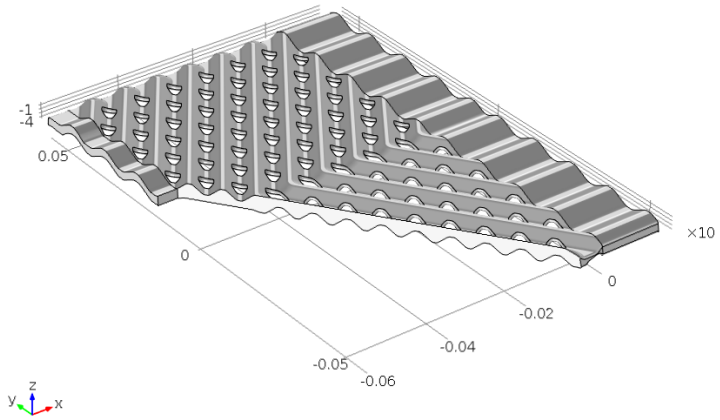

Figure 7. A representation of the distribution zone of one fluid channel domain, provided by SWEP International AB.

3.1.1 Simplified Viscosity Model

The geometry started as an inlet rectangle in a zy-work plane centered at the origin. This rectangle was extruded in the x-direction to form a block. A new zy-work plane was created at the end of the previous block. Two equally sized rectangles were built in this plane, matching the outer edges of the previous block but with a middle gap of 0.2 mm from each other. Both rectangles were extruded in the positive x-direction. The geometry was

mirrored at the end of the resulting flow channels to create an inlet region, two parallel channels and an outlet region according to Figure 8. The main flow direction is along the x-axis. Detailed information about the geometry can be seen in Table 1 where width, height and length refer to the z, y and x-axis respectively.

Mesh was built by dividing the domain into inlet, channel and outlet regions. The inlet and outlet region were further divided in two parts by zy-work planes placed 0.015 m from the inlet and outlet respectively. Finer mesh was created for the channel region and inlet/outlet region closest to the parallel channels due to large temperature and velocity gradients. *Coarse* mesh quality was chosen for the first inlet and last outlet region, and *normal* for the second inlet, first outlet and channel regions. Triangular prism boundary layers were defined inside the whole domain. Mesh details can be seen in Figure 9 and Table 2.

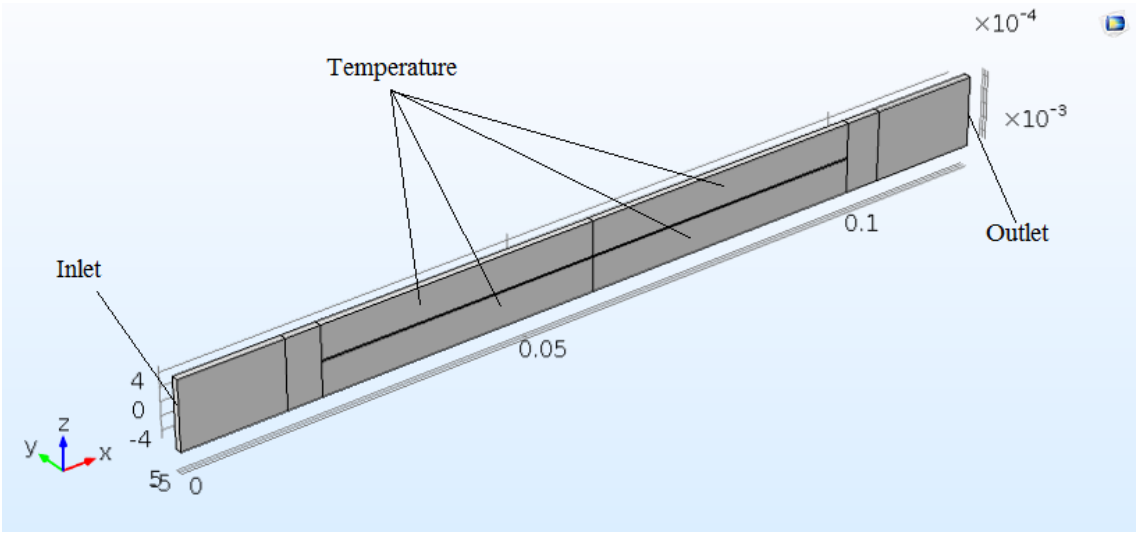

Figure 8. The geometry used for evaluation of viscosity effect on flow distribution including boundary condition clarifications.

Table 1. Dimensions used for building the model used for investigations of viscosity effects on flow distribution.

	Inlet/Outlet	Channels
Width(z) [m]	0.01	0.0049
Height(y) [m]	0.001	0.001
Length(x) [m]	0.02	0.04

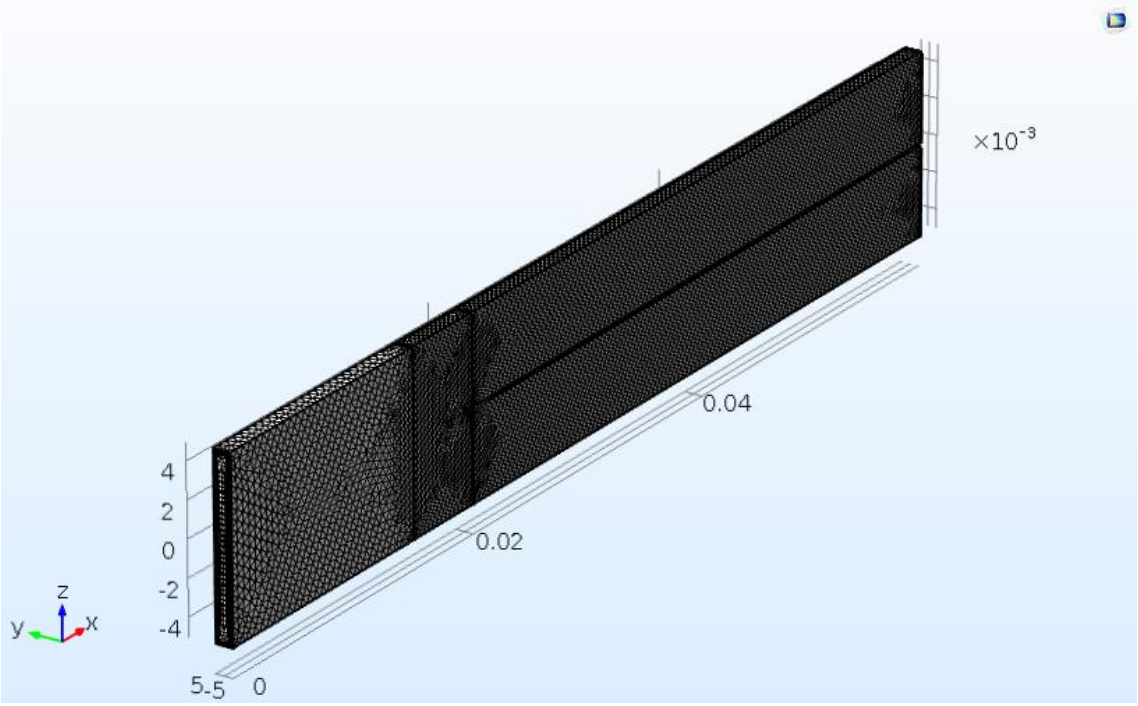

Figure 9. Resultant inlet and channel meshes including triangular prism boundary layers for the model used for viscosity investigations.

Table 2. Viscosity model mesh quality details, including boundary layers, in the viscosity investigation model.

Region	Total Mesh		Boundary Layers	
	Setting	Elements	Layers	Stretching factor
Inlet/Outlet	Coarse	66 174	8	1.2
Inlet/Outlet	Normal	61 473	8	1.2
Channel	Normal	460 381	8	1.2
Total	-	588 028	-	-

Gravity was defined as a *volume force* acting on the whole domain. Two boundary conditions were defined under the *heat transfer in fluids module*. The *temperature* condition was used at the inlet boundary closest in Figure 9 and the eight largest surfaces surrounding each channel. *Outflow* was defined at the end surface opposite to the inlet. Two boundary conditions were defined under the *laminar flow module*. *Inlet* was defined at the surface representing the inlet and *outlet* at the opposite end surface. Placements of t*emperature, inlet, outlet* and *outflow* boundary conditions are clarified in Figure 8.

3.1.2 Simplified Gravity and Reynolds Number Model

The gravity and Reynolds number model was built similarly to the viscosity model. A xy-work plane was defined at z-coordinate 0 and a rectangle was drawn. The rectangle was extruded in the positive z-direction to represent the inlet region. Two rectangles were drawn in a new xy-work plane at the end of the previous extrusion and extruded further in the positive z-direction. The two latter resultant blocks represent flow channels. One of these channels was extruded with a displacement in the positive x-direction to create an angle between it and the other channel. The displacement needed to create a wanted angle

depends on the angle and length of the straight channel. Since the starting rectangles have the same width, an increased angle decreases the angled channel cross-sectional area in the flow direction. To keep the cross-sectional area in the flow direction equal for both channels, the origin rectangle width was defined as a function of the straight channel width and the angle. The dimensions, both constant and angle dependent, are shown in Table 3.

Table 3. Constant and angle dependent dimensions for building the model used for investigation of gravity and Reynolds number effects on flow distribution.

Dimension	Inlet	Angled channel	Straight channel
Length(z)[m]	0.08	$0.32/\cos(\varphi)$	0.32
Width(x)[m]	$0.04 \cdot \tan(\varphi)$	$0.04/\cos(\varphi)$	0.04
Thickness(y)[m]	0.01	0.01	0.01
Displacement(x)[m]	-	$0.32 \cdot \tan(\varphi)$	-

Mesh for the gravity and Reynolds number model was built using the automatic mesh tool in COMSOL. The mesh setting was set to *normal* over the whole domain. Angled channel length varies with angle and therefore number of elements is angle dependent. Triangular prism boundary layers were defined to cover the whole inside of the domain. Mesh details for different angles can be seen in Table 4. Resulting geometry including mesh can be seen in Figure 10.

Figure 10. Resulting geometry including mesh used for evaluation of gravity and Reynolds number effects on flow distribution.

Table 4. Angle dependent mesh details for the gravity and Reynolds number model.

	Boundary Layers		Number of Elements			
Angle	**Quantity**	**Stretching factor**	**Inlet**	**Straight**	**Angled**	**Total**
5	8	1.2	89 182	189 479	191 359	470 020
15	8	1.2	63 785	127 709	132 973	324 467
30	8	1.2	44 006	86 774	99 775	230 555
45	8	1.2	36 315	61 214	86 624	184 153

The *volume force* condition was used on the whole domain to account for gravity effects. Two boundary conditions were manually defined under the *heat transfer in fluids* module. The *temperature* was defined at the inlet surface visible in Figures 10 and 11. *Outflow* was defined at both boundaries in the other end of the geometry. Two manually defined boundary conditions were used under the *laminar flow* module. *Inlet* and *outlet* conditions were defined at the same boundaries as *temperature* and *outflow*. Placements of t*emperature, inlet, outlet* and *outflow* boundary conditions are clarified in Figure 11.

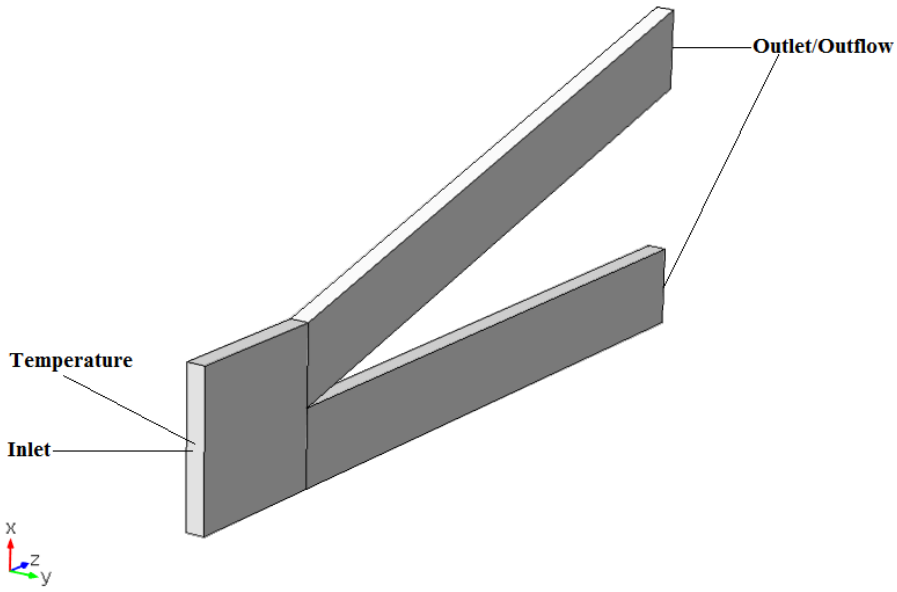

Figure 11. The geometry used for investigation of gravity and Reynolds number effects including a clarification of boundary conditions.

3.1.3 SWEP Distribution Zone Model

A more detailed model was provided by SWEP and also used in the study. This model was provided as a CAD-file. Simplifications were made by SWEP to fit this study's available hardware. The model represented the distribution zone in Figure 6, the part of the channel responsible for flow distribution over the heat transfer surface. The inlet port was replaced by an extended wavy block placed at one side of the flow channel. The outlet, on the opposite side, was replaced with an extended wavy block that stretched the whole width of the geometry. The zone between inlet and outlet represented the fluid domain created by the crossing chevron patterns of two plates. Brazed contact points were included and represented as holes in the fluid domain.

The CAD-file provided by SWEP was imported into COMSOL and converted into COMSOL-format. The geometry provided consisted of many surface fragments to approximate the wavy surfaces. Surface fragments were combined using the built-in tool *form composite faces* in COMSOL which decreased the number of surfaces from 4 214 to 95. Each region was basically transformed into top, bottom and side surfaces. The circular shape of the holes was approximated with several surfaces that were transformed into one surface for each hole. The resultant geometry is shown in Figure 12.

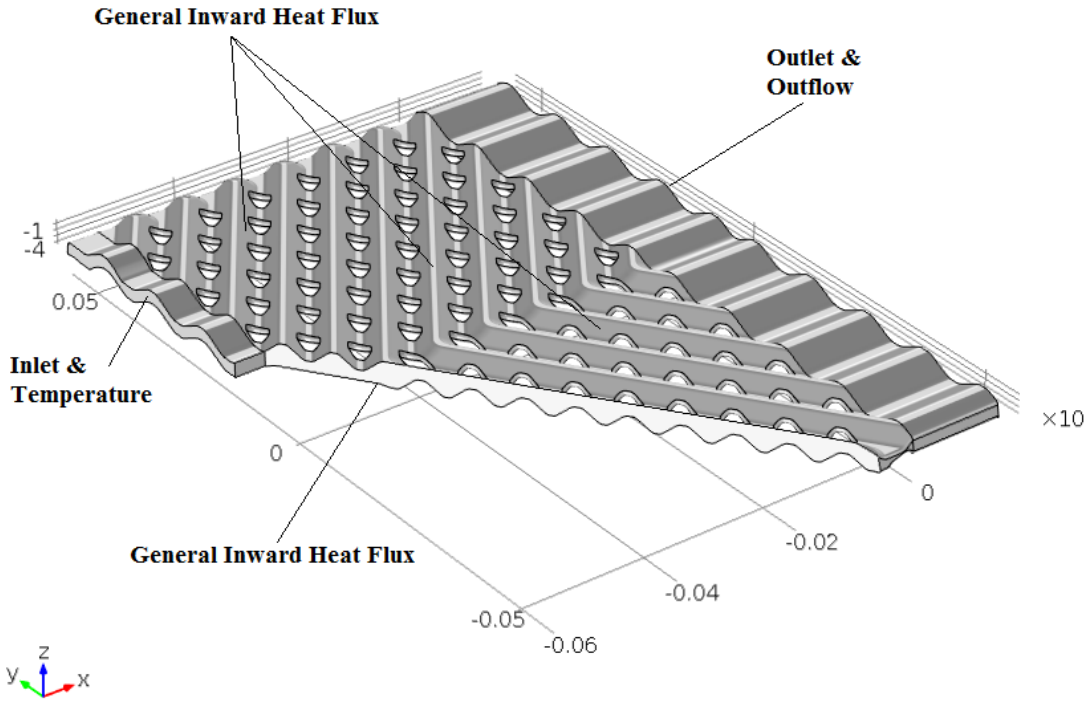

Figure 12. Model provided by SWEP after import and visual operations to make it easier to handle in COMSOL. Clarifications of boundary conditions are included.

Dimensions of the domain were not specified and had to be evaluated using *measure in* COMSOL. The inlet and outlet had an approximate width of 0.042 and 0.113 m respectively. The total length of the domain in the flow direction was approximately 0.076 m. Domain thickness varies over the domain due to the wavy surfaces. Meshing was done with the automatic mesh tool in COMSOL. The mesh has to be good enough to capture flow details created by the repetitive obstructions in the geometry. The automatic mesh setting was set to *coarser* and then gradually increased until the computations required more physical memory than available for this study. This resulted in a maximum mesh setting of *normal*. Eight triangular prism boundary layers were defined with a stretching factor of 1.25 for the whole domain excluding the inlet and outlet surfaces. The resulting mesh and the boundary layers can be seen in Figures 13 and 14.

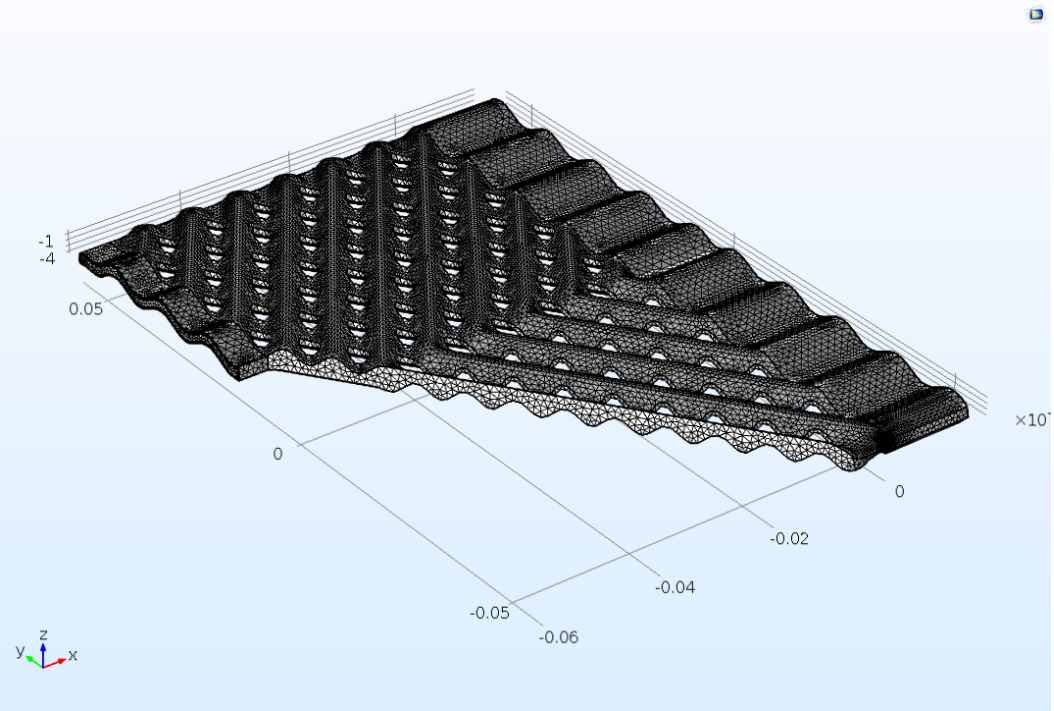

Figure 13. Resulting mesh at normal quality throughout the full size distribution domain.

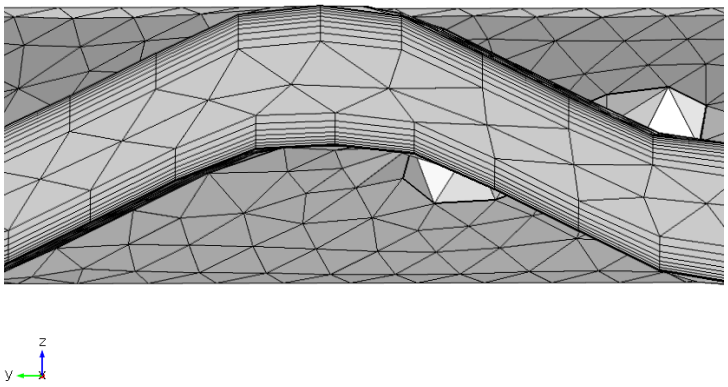

Figure 14. Inlet mesh including eight boundary layers at normal mesh quality for the full size distribution zone model.

A *volume force* was used on the whole domain to include gravity effects. Five boundary conditions were defined for the full size distribution geometry. For the *heat transfer in fluids* module, the *temperature* condition was used at the lowest horizontal and wavy surface in Figure 12 representing the inlet. In the opposite end surface of the geometry, the *outflow* condition was used. On the largest top and bottom surfaces of the perforated volume, seen in Figures 12 and 13, a negative *general inward heat flux* was defined to account for cooling effects. *Inlet* and *outlet* were defined at the same boundaries as *temperature* and *outflow*. *General inward heat flux, inlet, outlet,* and *outflow* boundary conditions are clarified in Figure 12.

3.2 Validation & Mesh Independence Study

This section contains a description of the validation and mesh independence study of the models used. Complex flow in plate heat exchangers makes real size models time-consuming and computationally expensive. Therefore, studies are advantageously made on simplified models where parameter influence can be isolated and investigated individually. However, models that do not fairly reflect reality are useless. Therefore, it must be proved that models follow the expected physical behavior. Since some of the models used in this study were created for this study alone, there is neither experimental validation data available nor a possibility to generate such data. This means that the validation in this study had to be made by physical expressions that describe the expected fluid behavior.

One thing that also affects the results generated by the model is the mesh quality since it is responsible for the number of nodes analyzed. It defines the quality, computational time as well as the required memory for the simulations. Therefore, it is necessary to check whether the mesh quality is good enough to capture fluid flow and heat transfer details or not. The mesh is considered good enough when a higher detail level does not noticeably alter the results. (COMSOL Inc. 2016b).

3.2.1 Simplified Viscosity Model

Piping networks generally contain junctions, series and parallel connections. Two principles lay the foundation for the analysis of piping systems. The mass conservation principle is fundamental when dealing with piping networks. Since fluids are considered incompressible, it is important that the mass balance is valid in every connection. Another principle states that pressure drop between two points is equal regardless of the path followed. Two parallel and later rejoining pipes have the same pressure drop regardless of the path between two fixed points. (Cengel & Cimbala 2010)

This pressure drop principle can be used to derive an expression for the pressure drop in two parallel pipes. The pressure drop inside a pipe of length L and hydraulic diameter D_h, can be described as a function of density (ρ), average velocity ($\overline{V}$) and the friction factor (f) (30). The friction factor for rectangular pipes is related to the Reynolds number depending on the width to height ratio of the channel in Table 5. For this case, the channel width is four times the height. The Reynolds number is calculated with the average velocity ($\overline{V}$), hydraulic diameter (D_h), density (ρ) and dynamic viscosity (μ) (31). Since the pressure loss of both channels should be equal, two pressure drop equations should equal each other, one for each channel (32). It is possible to simplify the expression due to the equal geometries of the parallel channels (33). By the definition of dynamic viscosity in Eq. 34 and multiplication by the cross sectional area on both sides, it is possible to relate the mass flow of the two channels to the kinematic viscosity (35). This means that mass flow depends on the kinematic viscosity.

Table 5. Friction factor in rectangular ducts is dependent of Reynolds number and width to height ratio. (Cengel & Cimbala 2010)

w/h	Friction Factor (f)
1	56,92/Re
2	62,20/Re
3	68,36/Re
4	**72,92/Re**
6	78,80/Re

$$\Delta P_L = f \frac{L}{D_h} \frac{\rho \bar{V}^2}{2} \tag{30}$$

$$\mathrm{Re} = \frac{\rho \bar{V} D_h}{\mu} \tag{31}$$

$$\Delta P_1 = \Delta P_2 \Rightarrow \frac{72.92 \cdot L_1 \mu_1}{D_{h1} \rho_1 \bar{V}_1} \frac{\rho_1 \bar{V}_1^2}{2} = \frac{72.92 \cdot L_2 \mu_2}{D_{h2} \rho_2 \bar{V}_2} \frac{\rho_2 \bar{V}_2^2}{2} \tag{32}$$

$$\mu_1 \cdot \bar{V}_1 = \mu_2 \cdot \bar{V}_2 \tag{33}$$

$$\mu = \nu \cdot \rho \tag{34}$$

$$\dot{m}_1 \cdot \nu_1 = \dot{m}_2 \cdot \nu_2 \Rightarrow \frac{\dot{m}_1}{\nu_2} = \frac{\dot{m}_2}{\nu_1} \tag{35}$$

$$V_1 \cdot \rho_1 \cdot \nu_1 = V_2 \cdot \rho_2 \cdot \nu_2 \tag{36}$$

Since mass flow is dependent of kinematic viscosity, the derived expression (35) was used to validate the simplified viscosity model. The flow channel areas are equal and after a rearrangement of terms, the expression can be written in another form (36). This expression (36) is easier to use due to the possibility to define the product of these terms along the same lines in COMSOL. Therefore, the product of velocity, density and kinematic viscosity (36) was evaluated along a central line through the hot and cold channel, and plotted in the same graph for comparison. The resulting two lines should be close to each other in the graph if the expected physical behavior is followed. Validation was made for both Shell Rimula 40 and water. Results from the validation process were also used for the mesh independence study. The automatic mesh tool was used and three adjacent mesh qualities were built. Each detail level step is approximately twice as good as the previous. Since the model was divided in two regions with different detail levels, the difference between them was kept constant as they were varied in the same direction. Settings used in the mesh independence study can be seen in Table 6. Validation results were compared for different mesh qualities.

Table 6. Mesh details from the mesh independence study of the simplified viscosity model.

	Inlet/Outlet	Channels	Number of Elements
Mesh 1	Coarser	Coarse	210 597
Mesh 2	Coarse	Normal	588 028
Mesh 3	Normal	Fine	1 129 354

3.2.2 Simplified Gravity and Reynolds Number Model

Validation of the gravity and Reynolds number model was based on the same expression for pressure loss as the simplified viscosity model. Pressure drop in a fluid channel (37) due to viscous effects is dependent of friction factor (f), density (ρ), average flow velocity ($\bar{V}$), channel length (L), and hydraulic diameter (D_h). Friction factor is determined from the channel width to height ratio as in the viscosity model (38). The resultant pressure drop correlation can be written as a function of channel length (L), average velocity ($\bar{V}$),

dynamic viscosity (μ), and hydraulic diameter (D_h) (39). Since the channel length increases frictional pressure drop, the pressure drop is higher in the angled flow channel for angles greater than zero. Therefore, it is not possible to equal the expressions for pressure loss in the individual channels as long as there is an angle between them. A ratio between pressure drops can be calculated instead. Such a ratio is dependent of channel length (L) and average velocity ($\overline{V}$) (40).

$$\Delta P_L = f \frac{L}{D_h} \frac{\rho \overline{V}^2}{2} \tag{37}$$

$$f = \frac{72{,}92}{\mathrm{Re}} = \frac{72{,}92 \cdot \mu}{\rho \cdot \overline{V} \cdot D_h} \tag{38}$$

$$\Delta P_L = \frac{72{,}92 \cdot L \cdot \overline{V} \cdot \mu}{D_h^2 \cdot 2} \tag{39}$$

$$\frac{\Delta P_1}{\Delta P_2} = \frac{\left(\frac{72{,}92 \cdot L_1 \cdot \overline{V}_1 \cdot \mu_1}{D_{h1}^2 \cdot 2} \right)}{\left(\frac{72{,}92 \cdot L_2 \cdot \overline{V}_2 \cdot \mu_2}{D_{h2}^2 \cdot 2} \right)} = \frac{L_1 \cdot \overline{V}_1}{L_2 \cdot \overline{V}_2} \tag{40}$$

The pressure loss ratio indicates an expected behavior of the system. The ratio of pressure losses in each channel should equal the ratio between the respective channel lengths and average velocities (40). Simulations were run with different input angles and the resultant pressure ratios were compared to the velocity and length ratios. Channel angle was used as input parameter which in turn gave different angled channel lengths. A mesh independence study was made for the gravity and Reynolds number model. Three steps of mesh quality were analyzed and compared to choose a mesh that captures flow behavior and minimizes computational times and memory requirements. The validation results were used for the comparison of mesh qualities. Since the length of the angled flow channel increases with angle, the mesh number of elements varies with both quality and angle. In this study, a sharper angle gave a higher number of elements. Investigated mesh qualities and their respective number of elements are listed in Table 7.

Table 7. Mesh details for different angles and automatic mesh quality for the simplified Reynolds number and gravity model.

Angle[°]	Number of Elements		
	Coarse	Normal	Fine
5	172 866	470 020	874 306
15	123 233	324 467	609 762
30	79 665	230 555	399 225
45	67 243	184 153	322 292

3.2.3 SWEP Distribution Zone Model

There was no experimental data available for validation of the model. Since the model represents a part of a plate heat exchanger channel, the temperature difference between inlet and outlet should be small. An assumption was made that a 10 °C cooling should be

achieved in the model based on a discussion with Patrik Gerenmark (2016). The heat flux necessary to achieve this was calculated with the inlet area (A_{inlet}), density (ρ_{inlet}), velocity (V_{inlet}), specific heat ($C_{p\text{-}inlet}$) and temperature difference (ΔT) of Shell Rimula 40 and water (41). A constant heat flux per area was defined as a boundary condition on both sides of the perforated domain between the inlet and outlet (42). Fluid velocities and properties were evaluated at the inlet, as viewed in Table 8. Inlet and heat transfer areas (A_{inlet}, A_{heat}) were evaluated using the built in *measure* tool in COMSOL and used for calculations. Simulated outlet temperature was compared to the expected 10 °C temperature difference for heat transfer validation.

$$q_{heat} = A_{inlet} \cdot \rho_{inlet} \cdot V_{inlet} \cdot C_{p-inlet} \cdot \Delta T \tag{41}$$

$$Q_{heat} = \frac{q_{heat}}{A_{heat}} \tag{42}$$

Fluid flow is more complex to validate in this kind of geometry. Since the inlet is placed on one side of the geometry, flow paths differ in length between inlet and outlet. Longer paths yield a lower fluid temperature since the heat flux is constant. Lower temperatures give higher viscosities and therefore higher resistances to fluid flow. A lower flow velocity is expected in the parts of the outlet furthest from the inlet. This theory together with the expected temperature difference of 10 °C was used for model validation.

Table 8. Fluid properties used for calculation of and resulting constant heat flux for a 10 °C cooling in the full size distribution model.

	T [°C]	V [m/s]	ϱ [kg/m^3]	A_{inlet} [m^2]	A_{heat} [m^2]	C_p [J/kg·°C]	ΔT [°C]	Q_{heat} [W/m^2]
SR40	90	0.5	850	$8.203 \cdot 10^{-5}$	0.008882	2 106	-10	-82 663
Water	90	0.5	965	$8.203 \cdot 10^{-5}$	0.008882	4 208	-10	-187 515

A mesh independence study was made together with the validation on the full size distribution model. Three different mesh qualities were used during the validation to investigate mesh dependency. Mesh qualities used can be seen in Table 9. In COMSOL, velocities and temperatures for the validation and mesh independence study were evaluated at points placed in the outlet region. A total of 18 points were placed along the width of the channel, 0.005 m from the outlet surface and at a z-coordinate corresponding to the mean value of the outlet domain fluctuations. The y-coordinates can be seen in Table 10. Velocities and temperatures were plotted as a function of mesh and y-coordinate for comparison. Shell Rimula 40 was used for validation and mesh independence study.

Table 9. Number of elements for the mesh qualities used in the combined mesh independence study and validation.

Mesh	Quality	Elements
1	Coarser	157 380
2	Coarse	247 367
3	Normal	454 313

Table 10. Y-coordinates of the points used for evaluating velocities and temperatures at the outlet region in the full size distribution model.

Point	**1**	**2**	**3**	**4**	**5**	**6**	**7**	**8**	**9**
y [m]	-0.05	-0.044	-0.038	-0.026	-0.02	-0.014	-0.012	-0.006	0
Point	**10**	**11**	**12**	**13**	**14**	**15**	**16**	**17**	**18**
y [m]	0.006	0.012	0.014	0.02	0.026	0.032	0.038	0.044	0.05

3.3 Parameter Study

The goal of a parameter study is to investigate the influence of each individual parameter on the main results. During the parameter study, it is wanted to keep all or as many other parameters as possible constant to isolate the influence of the respective parameter. The parameter investigation methods of this study are presented below.

3.3.1 Viscosity

Due to the close parallel between viscosity and flow behavior, it is interesting to see if and how viscosity affects the flow maldistribution between channels. Because of its temperature dependency, viscosity effects are easily investigated through introducing temperature differences between flow channels. Viscosity effects were investigated through definition of one hot and one cold channel in the simplified viscosity model. Three different degrees of temperature differences were defined and each channel mass flow was evaluated using post-processing tools in COMSOL. The mass flow was calculated with velocity (V), area (A) and density (ϱ) at the middle of both channels (43). Flow distribution in the hot and cold channel respectively, was calculated in percent of the total flow and compared (44). Simulations and calculations were made both for Shell Rimula 40 and water. Used temperature inputs can be seen in Table 11. The inlet velocity was kept constant at 0.05 m/s.

$$\dot{m}_i = V_i \cdot A_i \cdot \rho_i \tag{43}$$

$$\dot{m}_{\%i} = \frac{\dot{m}_i}{\dot{m}_{cold} + \dot{m}_{hot}} \cdot 100,\ i = cold, hot \tag{44}$$

Table 11. Temperature inputs used to investigate viscosity effects on flow distribution for Shell Rimula 40 and water.

Water/Shell Rimula 40				
	T_{inlet} [°C]	T_{hot} [°C]	T_{cold} [°C]	A_{cs}[m^2]
Case 1	20	60	55	$4.9 \cdot 10^{-6}$
Case 2	20	80	55	$4.9 \cdot 10^{-6}$
Case 3	20	100	55	$4.9 \cdot 10^{-6}$

3.3.2 Gravity

Gravity's effect on flow distribution was investigated with the simplified gravity and Reynolds number model. Gravity orientation was varied and the mass flow in both outlets was studied and compared. Velocities and densities were evaluated as surface averages on the outlet boundaries. Mass flow was calculated as in the viscosity case above. Since the main flow occurs in the xz-plane along the z-axis, gravity in the y-direction was neglected and not investigated. Investigated cases can be seen in Table 12. The inlet velocity and temperature were kept constant at 0.2 m/s, 80°C for oil and 20°C for water. No heat transfer occurred in these simulations. The 15° angle model was used for the investigations.

Table 12. Gravity orientations used for investigating gravity effect on flow distribution in the gravity and Reynolds number model.

	Fluid	Gravity Direction
Case 1	Water	+Z
Case 2	Water	-Z
Case 3	Shell Rimula 40	+Z
Case 4	Shell Rimula 40	-Z
Case 5	Shell Rimula 40	+X
Case 6	Shell Rimula 40	-X

3.3.3 Reynolds Number

A constant temperature means a constant density and viscosity in the domain, and also in the Reynolds number definition (45). Therefore, a variation of Reynolds number for a constant temperature domain is only possible through variation of hydraulic diameter (D_h) or average velocity ($\overline{V}$). Velocity was varied in this study and the mass flow rate was evaluated at each channel (43). The average channel velocity was used for the calculations and the mass flow was compared in percentage of total flow (44). The simplified gravity and Reynolds number model was used and the angle between flow channels was constant at 45°. Four different cases were investigated for each fluid, as can be seen in Table 13. As oil has a higher viscosity than water, flow velocity required for turbulence was unrealistic and not investigated. Half of the investigations for water were made on transitional and turbulent flow, and the other half on laminar. Turbulence occurs easier at the inlet due to the larger hydraulic diameter than in the channels. Therefore, the inlet section was used for determining whether turbulence occurred or not through the Reynolds number (45).

$$\mathrm{Re} = \frac{\rho \cdot \overline{V} \cdot D_h}{\mu} \tag{45}$$

Table 13. Cases simulated to investigate Reynolds number effects on flow distribution in the gravity and Reynolds number model.

SR40	T [°C]	ϱ [kg/m³]	μ[Pa·s]	$D_{h\text{-inlet}}$ [m]	V_{inlet} [m/s]	Re_{inlet} [1]	Flow
Case 1	80	856	0.02204	0.01812	0.05	35	Laminar
Case 2	80	856	0.02204	0.01812	0.1	70	Laminar
Case 3	80	856	0.02204	0.01812	0.2	141	Laminar
Case 4	80	856	0.02204	0.01812	0.4	282	Laminar
Water							
Case 1	20	998.2	0.001	0.01812	0.05	904	Laminar
Case 2	20	998.2	0.001	0.01812	0.1	1809	Laminar
Case 3	20	998.2	0.001	0.01812	0.2	3617	Transitional
Case 4	20	998.2	0.001	0.01812	0.4	7235	Turbulent

3.4 SWEP Distribution Zone Model

Parameter studies on simplified geometries can be useful for evaluating effects of individual parameters. However, it may prove difficult to predict the behavior of a real case based on the simplified conditions. When parameters of interest have been identified, they can be further investigated with models that are more reminiscent of reality. A model that represents a complete BPHE is too computationally expensive for the available hardware. A simplified but yet detailed model of a flow distribution zone was provided by SWEP for

this study. The model was used for further investigations of the parameters evaluated in the simplified models.

3.4.1 Viscosity

Viscosity effects were evaluated through temperature differences due to the temperature dependency of viscosity. A constant heat flux per area was defined at both sides of the perforated middle domain to achieve a specific degree of fluid cooling. As mentioned in the validation, the necessary heat flux (41) depends on mass flow, heat capacity and wanted temperature difference. Heat transfer area was evaluated using COMSOL's *measure* tool, and used for defining the heat flux per area (42). Shell Rimula 40 was investigated at two different temperature differences and water was investigated at one for comparison. Gravity was neglected in the investigations, and inlet velocity and temperature where kept constant. Since the properties of oil and water differ, required heat flux differs between cases. Detailed fluid properties together with calculated heat flux can be seen in Table 14. Flow distribution was evaluated at the 18 points from the validation process of the same geometry. Flow velocities were evaluated at these points for all cases and plotted as a function of y-coordinate in the same graph.

Table 14. Fluid properties and resulting heat flux to achieve a specified temperature difference in the full size distribution model.

Fluid	T_{inlet} [°C]	V_{inlet} [m/s]	ϱ_{inlet} [kg/m^3]	A_{inlet} [m^2]	A_{heat} [m^2]	$C_{p-inlet}$ [J/kg·°C]	ΔT [°C]	Q_{heat} [W/m^2]
SR40	90	0.5	850	$8.203 \cdot 10^{-5}$	$8.9 \cdot 10^{-3}$	2 106	-10	-82 663
SR40	90	0.5	850	$8.203 \cdot 10^{-5}$	$8.9 \cdot 10^{-3}$	2 106	-5	-41 331
Water	90	0.5	965	$8.203 \cdot 10^{-5}$	$8.9 \cdot 10^{-3}$	4 208	-10	-187 515

3.4.2 Gravity

Gravity effects on flow distribution were evaluated by varying the orientation of gravity. Plate heat exchanger packages are generally oriented such that flow and gravity occur in the same or direct opposite directions. Both negative and positive x-direction was simulated since they correspond to these orientations. Inputs, such as inlet temperature, inlet velocity and heat flux, were kept constant during the investigations. Outlet velocity was plotted at 18 points as a function of y-coordinate. Results of no gravity and both x-directions were compared to each other. Input to the investigations can be seen in Table 15. The 10°C case with no gravity was plotted in the same graph for comparison. A gravity direction perpendicular to flow direction was not investigated due to simulation convergence problems.

Table 15. Cases investigated with respective inputs to investigate gravity effects on flow distribution in the full size distribution model.

Fluid	T_{inlet} [°C]	V_{inlet} [m/s]	ΔT [°C]	Q_{heat} [W/m^2]	Gravity Direction
SR40	90	0.5	-10	-82 663	+X
SR40	90	0.5	-10	-82 663	-X
SR40	90	0.5	-10	-82 663	-

3.4.3 Reynolds Number

Reynolds number effects on flow distribution were investigated by varying inlet velocity. Three cases were studied with different inlet velocities for Shell Rimula 40. Resulting Reynolds number for these three cases was calculated to examine the flow regime. Reynolds number calculations were made at the region of the perforated domain closest to the inlet with the smallest possible cross-sectional area. According to SWEPs definition of Reynolds number (46), narrower channel increases the risk of turbulence. This definition of Reynolds number was used since it is better adapted to this kind of geometry. Mass flow through the geometry was calculated with fluid inlet properties and velocity (47). The inlet area was evaluated using the *measure* tool in COMSOL. Resulting Reynolds numbers and model inputs for the different cases can be seen in Table 16. The temperature difference and gravity direction were kept constant at -10 °C and +X respectively.

$$\mathrm{Re}_{SWEP} = \left(\frac{\dot{m} \cdot 2}{w_{inlet} \cdot \mu_{inlet}} \right) \tag{46}$$

$$\dot{m} = \rho_{inlet} \cdot A_{inlet} \cdot v_{inlet} \tag{47}$$

Table 16. Model inputs, and calculation parameters for Reynolds number investigations of the full size distribution zone model.

	T [°C]	ϱ_{inlet} [kg/m^3]	v_{inlet} [m/s]	A_{inlet} [m^2]	$\dot{m}$ [kg/s]	w_{inlet} [m]	μ_{inlet} [Pa·s]	Re_{SWEP} [1]	Regime
1	90	850	0.25	$8.2 \cdot 10^{-5}$	0.0174	0.0422	0.0162	128	Laminar
2	90	850	0.5	$8.2 \cdot 10^{-5}$	0.0349	0.0422	0.0162	256	Laminar
3	90	850	1.0	$8.2 \cdot 10^{-5}$	0.0697	0.0422	0.0162	512	Laminar

4 Results

4.1 Validation & Mesh Independence Study

4.1.1 Simplified Viscosity Model

Results of both the validation and mesh independence study are presented in Figure 15. Regardless of fluid, it can be seen that the product of velocity, density and kinematic viscosity (35) are similar until the flow reaches the division at x-coordinate 0.02 m. A sudden spike in difference is observed at this point. This difference is temporary and decreases as the flow continues further into the parallel channels. The spike in difference is due to the larger velocity close to the hot channel, while the temperature and kinematic viscosity are unchanged. The difference fades faster for water than for Shell Rimula 40. If this dividing zone is neglected, the flow behavior is equal to such a level that the model is considered validated for further use.

A mesh independence study was made. It can be seen in Figure 15 that the product of velocity, density and kinematic viscosity varies with mesh for oil and water. The variations are larger for oil than water. For water, the results show a greater independency of mesh. Shell Rimula 40 results vary noticeably from the coarsest to middle mesh quality step. Variations from the middle step to the last are small in comparison to each other. An optimal mesh generates quality results as well as minimizes computational requirements. The increase in computational time from the middle to the last step was large, the middle mesh was chosen for further studies. This mesh consisted of *normal* quality in the channels and *coarse* quality at the inlet and outlet respectively. It was judged to fairly capture the flow behavior at a reasonable computational expense.

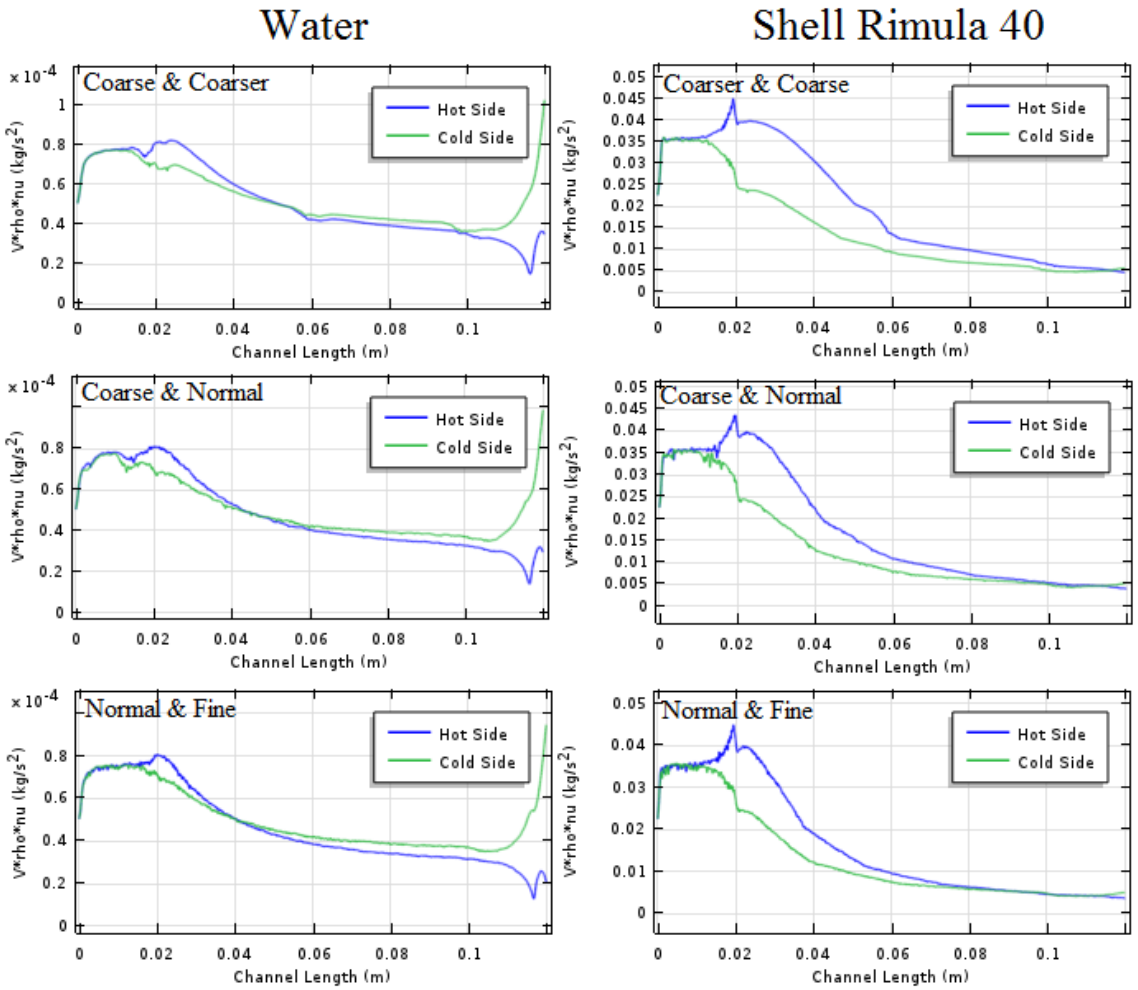

Figure 15. The product of velocity, density and kinematic viscosity (35) for lower to higher mesh settings for water and Shell Rimula 40 used for validation and mesh independence study.

4.1.2 Simplified Gravity & Reynolds Number Model

Resulting pressure drop ratios are compared to the velocity and length ratios in Table 17 and Figures 16, 17 and 18. Normal mesh quality, in Figure 17 and Table 17, was chosen for validation as explained later in this section. Small angles between flow channels result in better agreement between compared ratios than large angles. The absolute difference between ratios increases with increasing angle. Due to other effects introduced when the angle is increased, such as minor losses, the results show that the expected flow behavior is followed. The model was considered validated for further use.

As for the viscosity model, a mesh independence study was made together with the validation. The difference between pressure drop ratios and velocity and length ratios was investigated as a function of increased angle and mesh quality. The results of the mesh independence study can be seen in Table 17 and in Figures 16 to 18. Large fluctuations occur for *coarse* mesh quality and there is no clear error trend with angle. As the mesh quality is increased, these fluctuations disappear and the difference increases more linear with angle. When the mesh is increased from normal to fine, there is an increase in error for the lower angles and a decrease for high angles. Fine mesh leads to better quality but also to long computational times and high memory requirements that impinge on the

available hardware. The normal mesh quality was considered enough for this parameter study.

Table 17. Pressure drop ratios are compared to length and velocity ratios for different angles and mesh qualities to validate the gravity and Reynolds number model and to investigate mesh dependency.

Coarse Quality				
Angle [°]	$\frac{\Delta P_1}{\Delta P_2}$ [1]	$\frac{L_1 \cdot \bar{V}_1}{L_2 \cdot \bar{V}_2}$ [1]	Error [1]	Comp. time
5	0.999954	1.100021	0.100067	5 min 42 s
15	1.000901	0.9903	0.010601	4 min 37 s
30	1.004787	1.060407	0.05562	3 min 47 s
45	1.013084	0.905112	0.107971	3 min 3 s
Normal Quality				
5	1.000228	0.999616	0.000611	17 min 31 s
15	1.000741	0.993824	0.00689	9 min 44 s
30	1.004767	1.079666	0.074899	11 min 4 s
45	1.013297	0.9000582	0.112716	5 min 53 s
Fine Quality				
5	1.000146	0.994246	0.0059	1 h 11 min
15	1.001084	0.992565	0.008519	56 min 22 s
30	1.00469	1.056142	0.051451	20 min 38 s
45	1.013752	0.924903	0.08885	15 min 51 s

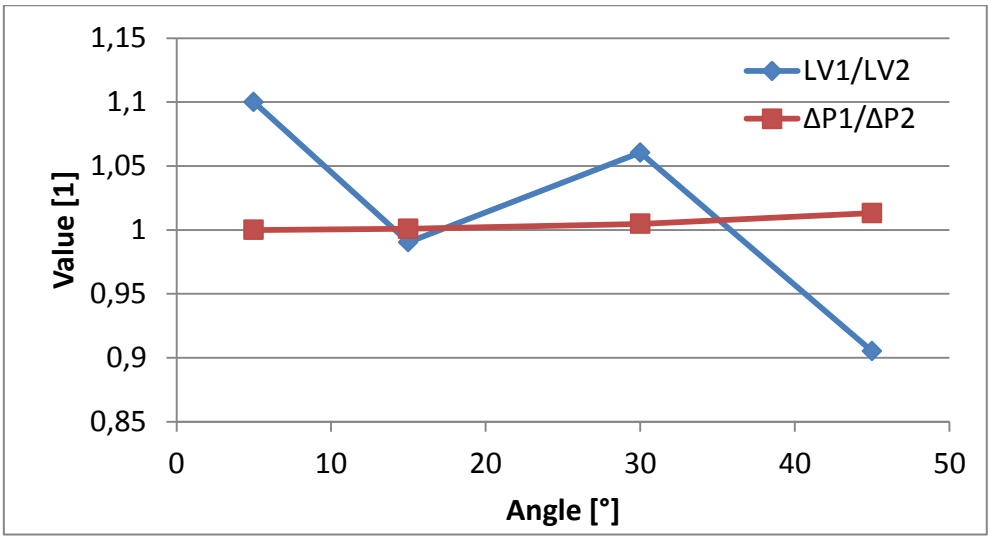

Figure 16. Gravity and Reynolds number model pressure drop ratios compared to velocity and length ratios for different angles at Coarse mesh quality.

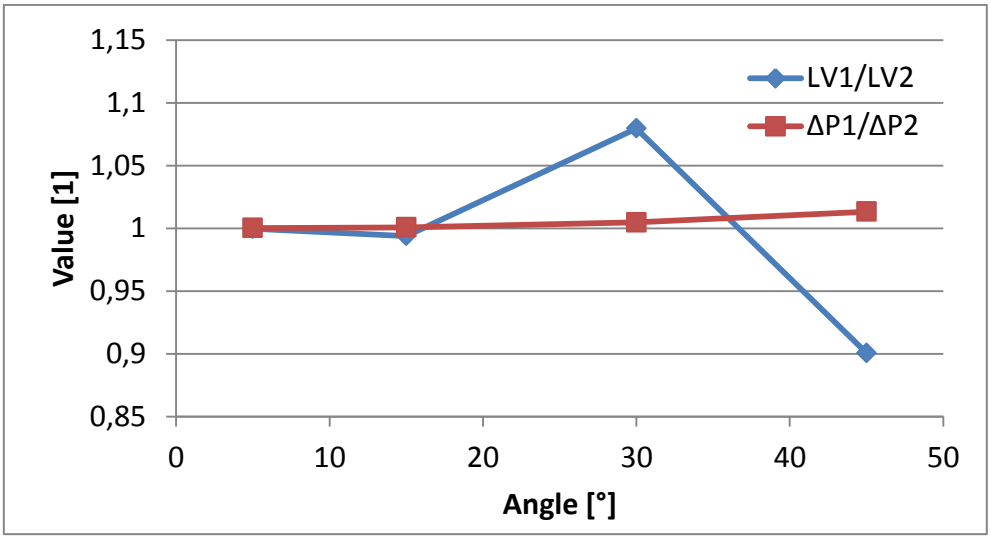

Figure 17. Gravity and Reynolds number model pressure drop ratios compared to velocity and length ratios for different angles at Normal mesh quality.

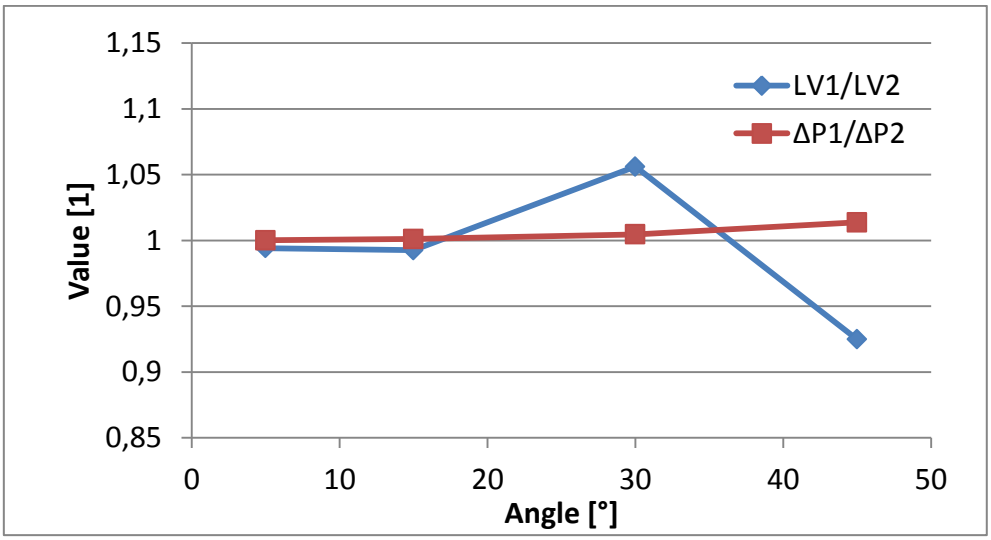

Figure 18. Gravity and Reynolds number model pressure drop ratios compared to velocity and length ratios for different angles at Fine mesh quality.

4.1.3 Full Size Distribution Model

Resulting temperatures and velocities for different y-coordinates and meshes can be seen in Figures 19 and 20. The agreement was considered good judged by the overall graphical behavior. Differences in singular points occur, especially in Figure 19. A difference between *coarser* and *coarse* mesh is noticeable, particularly in the velocity graph. The difference is noticeable but tolerable when mesh is increased from *coarse* to *normal*. A *fine* mesh was generated but was impossible to run since the number of elements exceeded the available computer capacity. *Normal* mesh was chosen for the simulations since it was considered good enough and it was impossible to increase the mesh quality further.

A *surface average* in COMSOL returned an average temperature of 77.7 °C at the outlet boundary, which corresponds to a domain temperature difference of 12.3 °C. About half the points in Figure 20 lie close to a temperature difference of 10 °C that was expected. The other half has differences between 11°C and 28 °C. This is a result of a constant heat flux defined from the domain and the longer flow paths to these points. The model was considered validated based on these results.

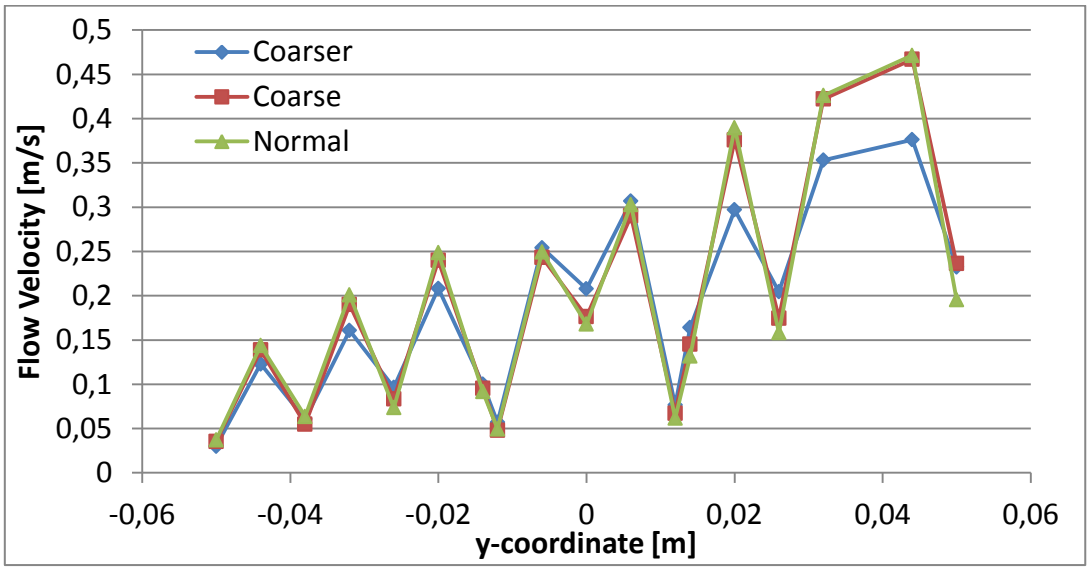

Figure 19. Outlet flow velocity at different y-coordinates and for different mesh qualities in the full size distribution model.

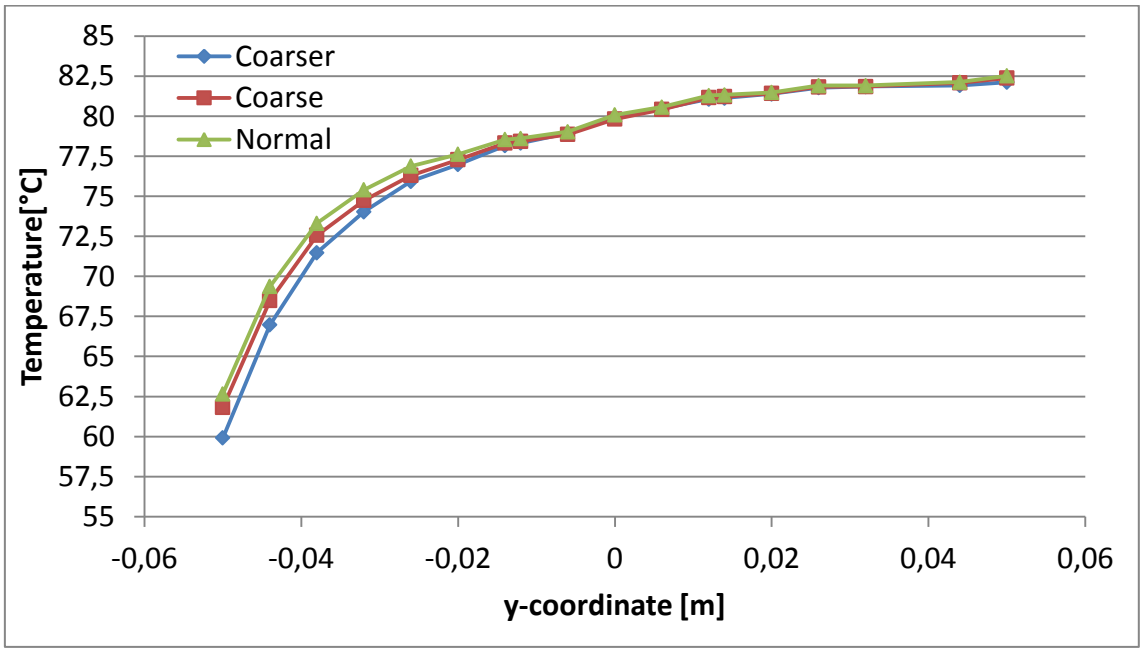

Figure 20. Outlet temperatures at different y-coordinates and for different mesh qualities in the full size flow distribution model.

4.2 Parameter Study

This section presents results generated from the simplified models. It is divided into sections for each parameter investigation.

4.2.1 Viscosity

The velocity magnitude and temperature distribution from the three investigated viscosity cases are presented in Figures 21, 22 and 23. It is visible that the cold channel velocity stays constant at approximately 0.5 m/s as the hot channel velocity increases with temperature. A higher velocity is observed close to the dividing region where the temperature is equal to the inlet temperature. Two zones of different velocities and temperatures are created at the outlet due to low mixing in laminar flow.

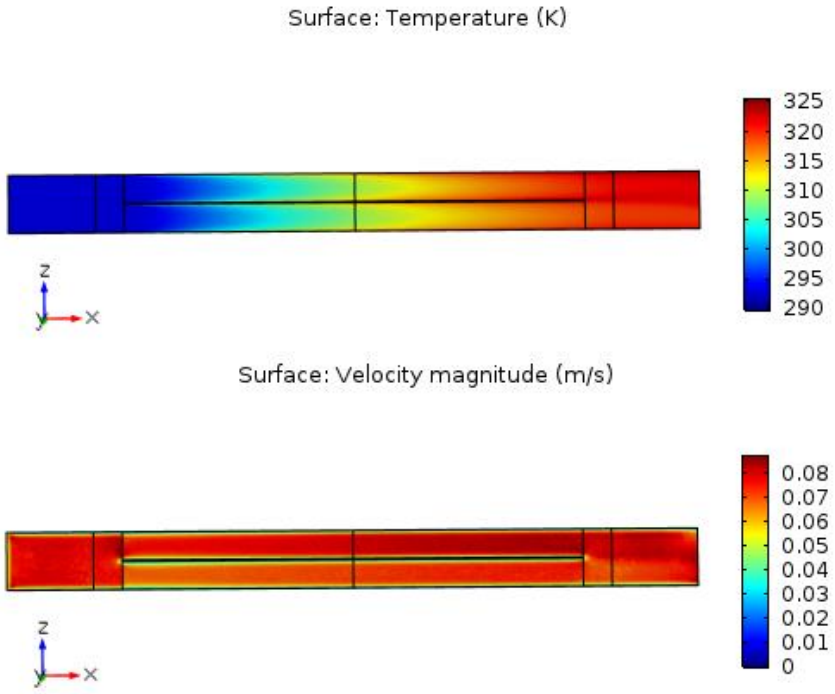

Figure 21. Shell Rimula 40 velocity magnitude and temperature distribution for the simplified viscosity model with a top channel temperature of 60 °C and a bottom channel temperature of 55°C.

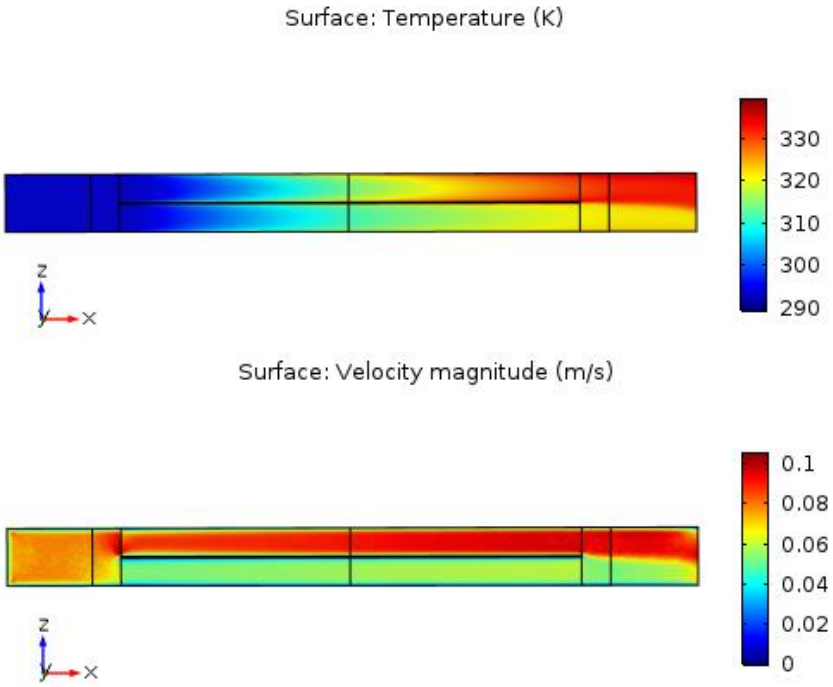

Figure 22. Shell Rimula 40 velocity magnitude and temperature distribution for the simplified viscosity model with a top channel temperature of 80 °C and a bottom channel temperature of 55°C.

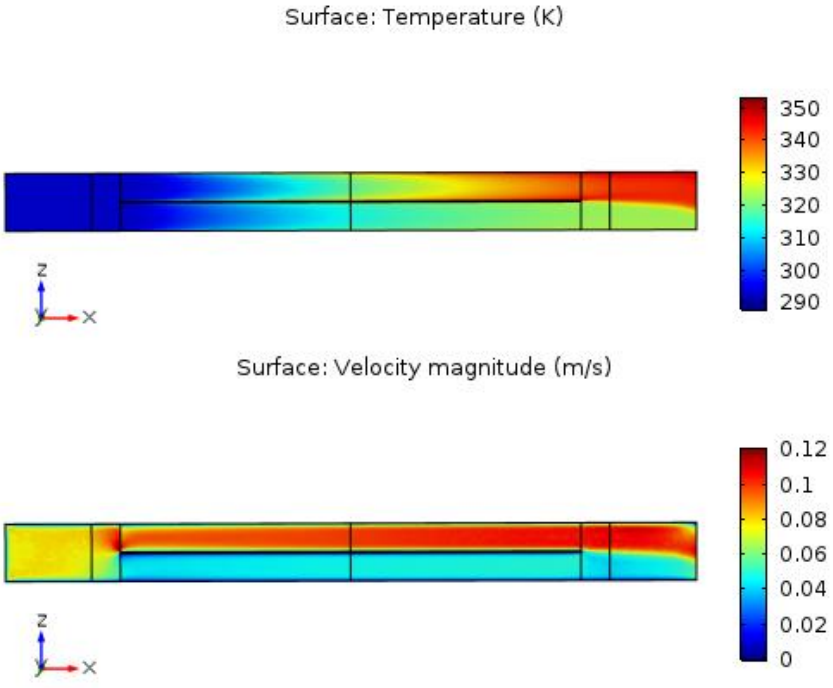

Figure 23. Shell Rimula 40 velocity magnitude and temperature distribution for the simplified viscosity model with a top channel temperature of 100 °C and a bottom channel temperature of 55°C.

Results from the viscosity investigations can be seen in Table 18 and are clarified in Figures 24 and 25. The difference in kinematic viscosity increases with temperature difference. A relationship between viscosity difference and mass flow distribution is noticeable for both Shell Rimula 40 and water. Flow maldistribution is initially small but increases linearly with increasing viscosity difference. This gets especially clear in the case of oil where a temperature difference results in a larger difference between kinematic viscosities and therefore also a larger flow maldistribution. In a plate heat exchanger, this means that for the same working temperatures, the risk of maldistribution is larger for oil than for water.

Table 18. Properties evaluated at the middle of the hot and cold channel and their calculated mass flow in percent to total flow.

	ν [m²/s]		**P [kg/m³]**		**V [m/s]**		$\dot{m}_i/\dot{m}_{tot}$ **[%]**	
Shell Rimula 40								
	Hot	Cold	Hot	Cold	Hot	Cold	Hot	Cold
Case 1	$1.32\cdot10^{-4}$	$1.43\cdot10^{-4}$	878.17	879.23	0.0528	0.04651	53.14	46.86
Case 2	$8.98\cdot10^{-5}$	$1.24\cdot10^{-4}$	872.74	877.94	0.0629	0.03654	63.11	36.89
Case 3	$6.52\cdot10^{-5}$	$1.12\cdot10^{-4}$	867.5	876.84	0.0697	0.02984	69.80	30.20
Water								
Case 1	$5.51\cdot10^{-7}$	$5.83\cdot10^{-7}$	988.89	990.41	0.05062	0.04891	50.82	49.18
Case 2	$4.48\cdot10^{-7}$	$5.76\cdot10^{-7}$	981.93	990.11	0.05465	0.04495	54.66	45.34
Case 3	$3.74\cdot10^{-7}$	$5.70\cdot10^{-7}$	973.89	989.89	0.05806	0.04163	57.84	42.16

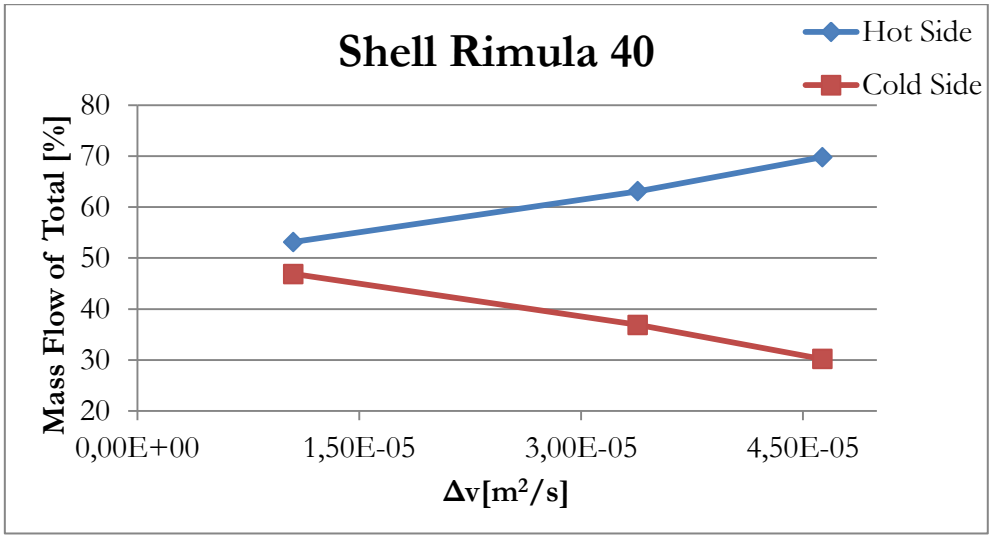

Figure 24. Shell Rimula 40 mass flow distribution between the hot and cold channel as the kinematic viscosity difference is increased.

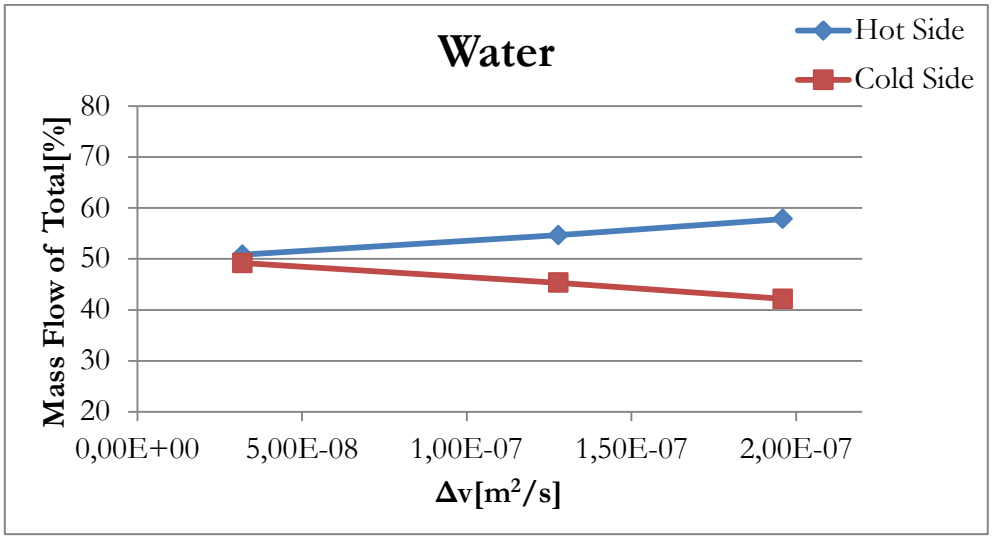

Figure 25. Water mass flow distribution between a hot and cold channel as the kinematic viscosity difference is increased.

4.2.2 Gravity

Shell Rimula 40 velocity magnitude for different gravity orientations in the gravity and Reynolds number model is presented in Figure 26. Both z-directions have identical velocity distributions with only a slight maldistribution between the angled and straight channel. A clear difference can be seen as gravity is put in the positive or negative x-direction. Almost no flow occurs in the channel placed in the opposite direction of gravity.

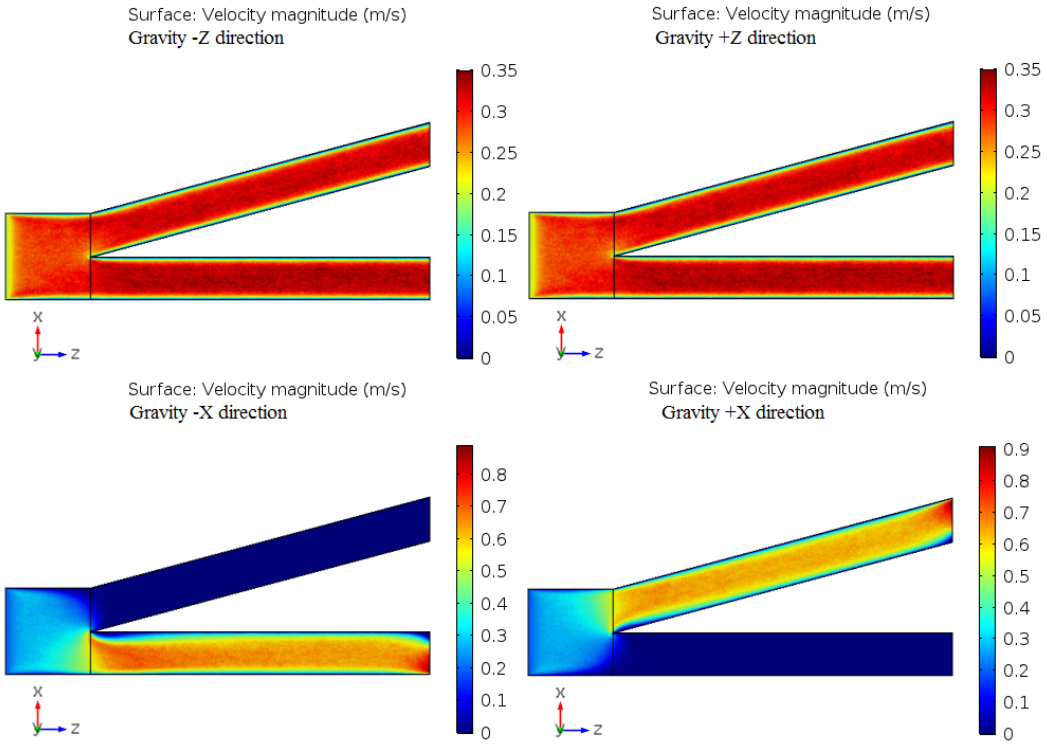

Figure 26. Resulting channel velocities of Shell Rimula 40 when gravity orientation is varied between negative and positive z and x directions.

Detailed results of varied gravity orientations can be seen in Table 19. When gravity acts along or counteracts the main flow direction, the z-direction, there is no change in flow distribution. The mass flow through the straight leg is slightly higher than the angled leg and this relation is kept constant even when the gravity orientation is put in the opposite direction. This result is valid for both water and Shell Rimula 40. When gravity orientation was perpendicular to the main flow direction, a large difference in flow distribution was noticed. More than 90 percent of the flow goes through the channel in the gravity direction despite the small angle of 15°. This result indicates that gravity affect flow distribution but only significantly if a height difference is introduced between flow paths in a flow channel.

Table 19. Properties used for calculation and the resulting mass flow distribution in percent as the gravity orientation was varied for Shell Rimula 40 and water.

Shell Rimula 40						
Gravity Direction	A [m^2]	ϱ [kg/m^3]	$\overline{V}_{angled}$ [m/s]	$\overline{V}_{straight}$ [m/s]	$\frac{\dot{m}_{angled}}{\dot{m}_{tot}}$ [%]	$\frac{\dot{m}_{straight}}{\dot{m}_{tot}}$ [%]
-Z	$4 \cdot 10^{-4}$	856	0.313	0.326	48.98	51.02
+Z	$4 \cdot 10^{-4}$	856	0.313	0.326	48.98	51.02
-X	$4 \cdot 10^{-4}$	856	0.0577	0.634	8.343	91.66
+X	$4 \cdot 10^{-4}$	856	0.646	0.0551	92.14	7.857
Water						
-Z	$4 \cdot 10^{-4}$	999.6	0.249	0.253	49.55	50.45
+Z	$4 \cdot 10^{-4}$	999.6	0.249	0.253	49.55	50.45

4.2.3 Reynolds Number

Velocity distributions for Shell Rimula 40 at four different inlet velocities are presented in Figure 27. It is hard to draw any conclusion about flow distribution from these figures since the ratio between velocities is kept intact. A lower velocity zone can be observed on the right side at the start of the angled channel. The flow velocity is higher in the straight channel than in the angled for all inlet velocities, and a high velocity zone stretches towards the inlet.

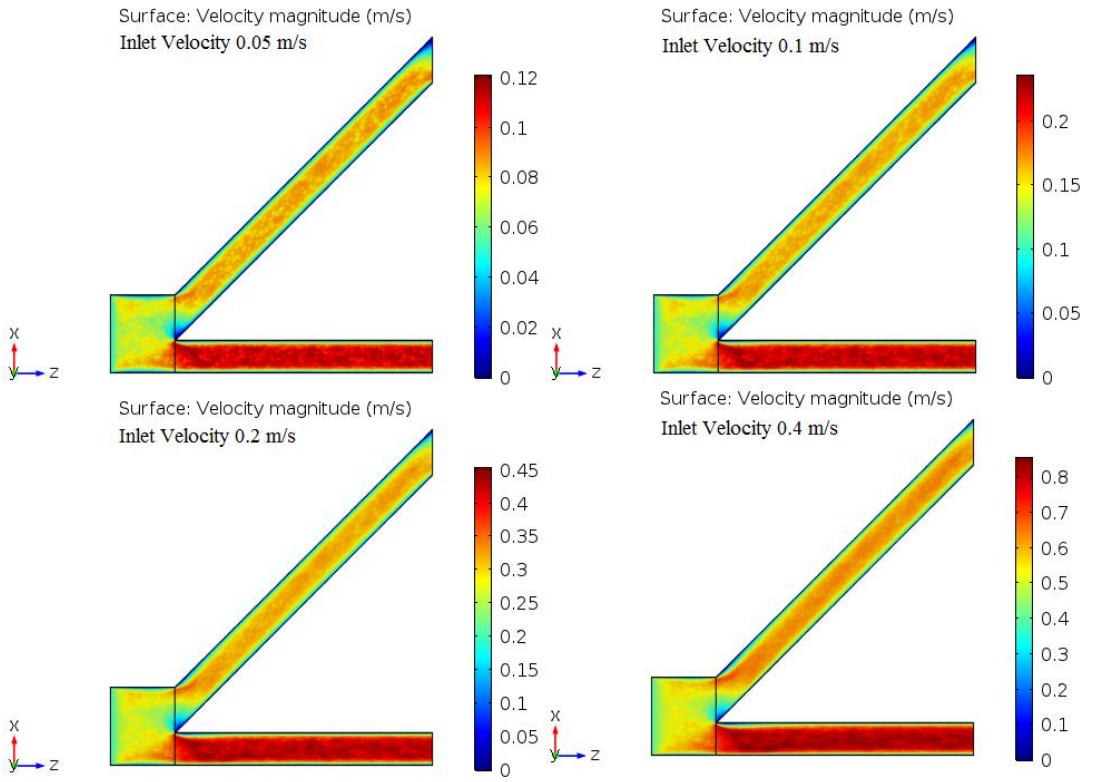

Figure 27. Velocity distribution of Shell Rimula 40 as the inlet velocity is increased in four steps from 0.05 to 0.4 m/s in the Reynolds number investigation.

Four different velocities were investigated for Shell Rimula 40 and water respectively. These resulted in four laminar cases for Shell Rimula 40, but two laminar and two turbulent cases for water. Resulting average velocities and flow distributions can be seen in Table 20 and Figures 28 and 29. At low inlet velocities, there is a larger flow maldistribution for both fluids. The maldistribution decreases as the inlet velocity increases. It is also visible in Table 20 and Figures 28 and 29 that flow maldistribution is smaller for water than for Shell Rimula 40. This is shown as a smaller gap between the curves in Figure 29 than in Figure 28. This indicates that a higher Reynolds number has a positive effect on flow distribution.

Table 20. Properties used and the calculated mass flow distribution in percent of total flow as the inlet velocity is varied for Shell Rimula 40 and water respectively in the Reynolds number investigation.

Shell Rimula 40						
V_{inlet} [m/s]	A [m^2]	P [kg/m^3]	$\bar{V}_{angled}$ [m/s]	$\bar{V}_{straight}$ [m/s]	$\frac{\dot{m}_{angled}}{\dot{m}_{tot}}$ [%]	$\frac{\dot{m}_{straight}}{\dot{m}_{tot}}$ [%]
0.05	$4 \cdot 10^{-4}$	856	0.0613	0.104	36.99	63.01
0.1	$4 \cdot 10^{-4}$	856	0.126	0.204	38.15	61.85
0.2	$4 \cdot 10^{-4}$	856	0.252	0.396	38.91	61.09
0.4	$4 \cdot 10^{-4}$	856	0.508	0.756	40.18	59.82
Water						
0.05	$4 \cdot 10^{-4}$	999.6	0.0636	0.0851	42.74	57.26
0.1	$4 \cdot 10^{-4}$	999.6	0.126	0.160	44.06	55.94
0.2	$4 \cdot 10^{-4}$	999.6	0.251	0.306	45.11	54.89
0.4	$4 \cdot 10^{-4}$	999.6	0.502	0.594	45.81	54.19

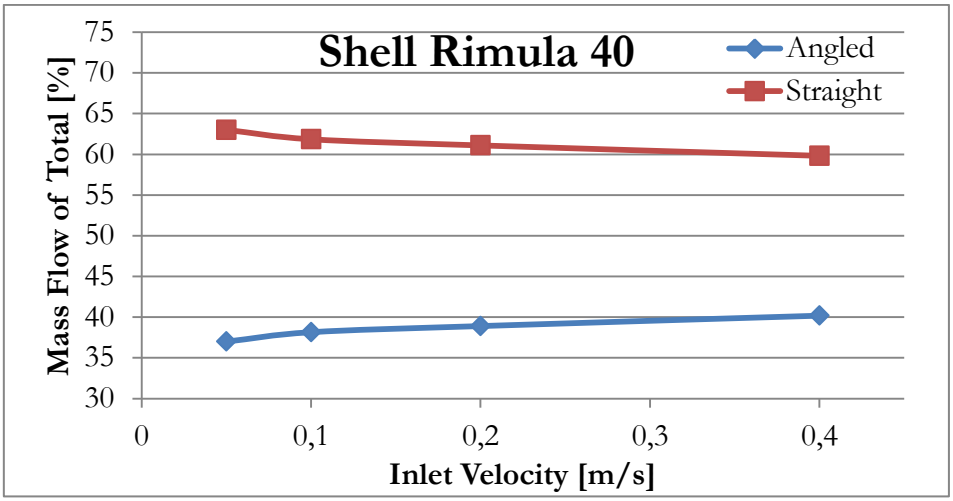

Figure 28. Mass flow distribution in percent of total flow for Shell Rimula 40 at different inlet velocities in the Reynolds number investigation.

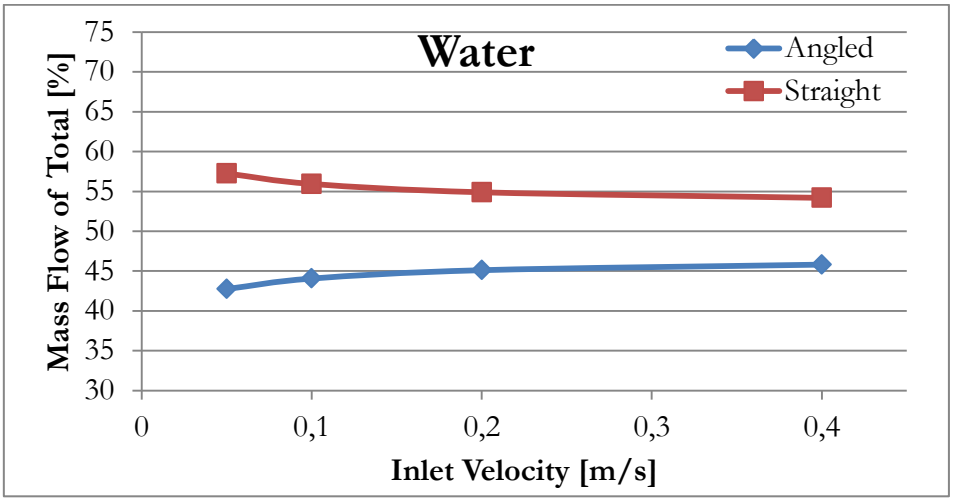

Figure 29. Mass flow distribution in percent of total mass flow for water at different inlet velocities in the Reynolds number investigation.

4.3 SWEP Full Size Model

Resulting velocity streamlines and temperature distribution for a chosen case are presented in Figures 30, 31 and 32. The Figures are taken from the Reynolds number investigations of the same geometry with inlet velocity 0.5 m/s. Based on the streamlines, it is possible to observe a flow maldistribution over the outlet boundary. Flow velocity is higher on the inlet side of the geometry which in turn means a higher mass flow. Acceleration zones are visible as the flow is forced to move around the braze points. The streamlines indicated helical flow paths as the lower right corner in Figure 30 is examined in Figure 31. The temperature distribution is uniform, except for the flow paths furthest from the inlet where a much lower temperature is observed.

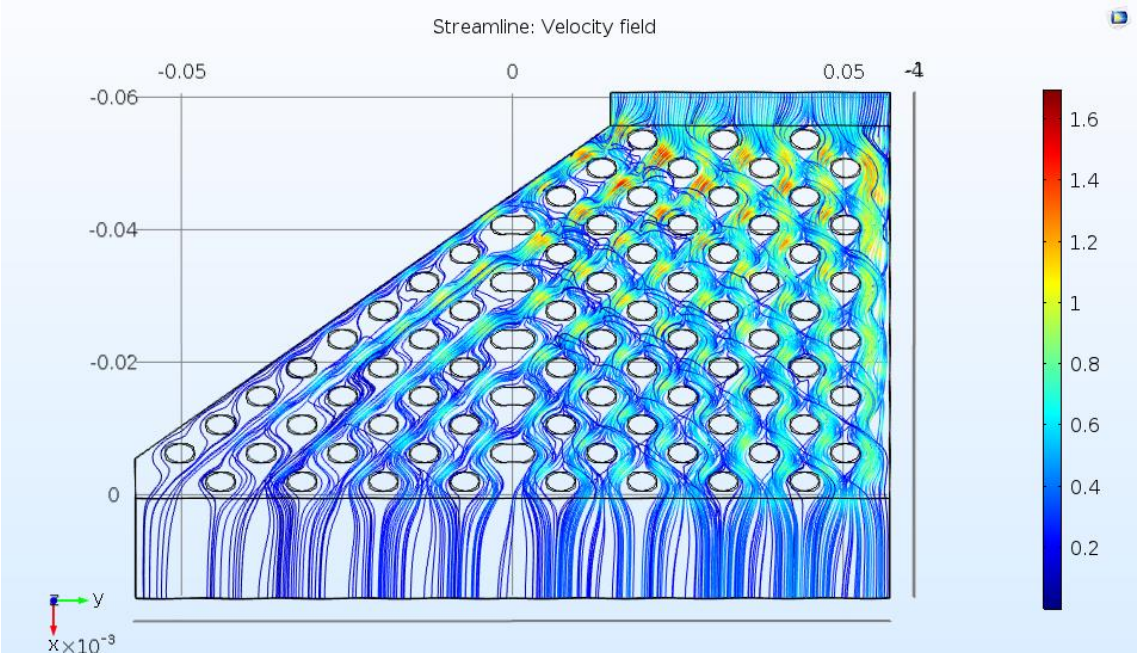

Figure 30. Velocity streamlines in the full size model for the Reynolds number investigations at inlet velocity 0.5 m/s.

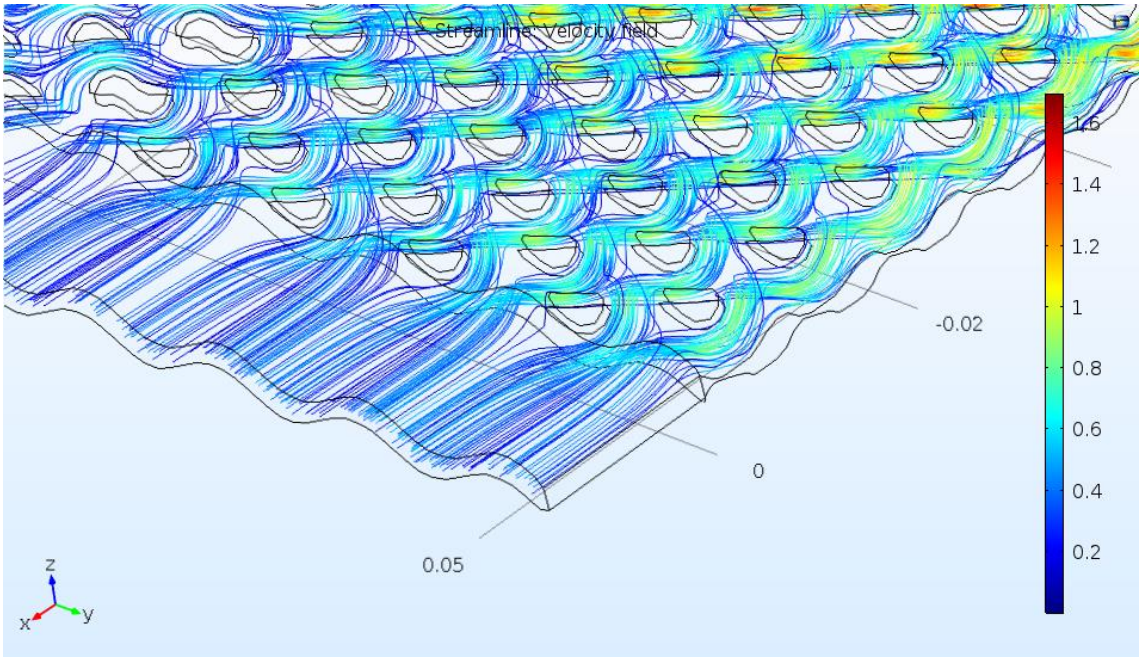

Figure 31. Velocity streamlines follow helical paths in the full size model as can be seen when examining the lower right corner of Figure 30.

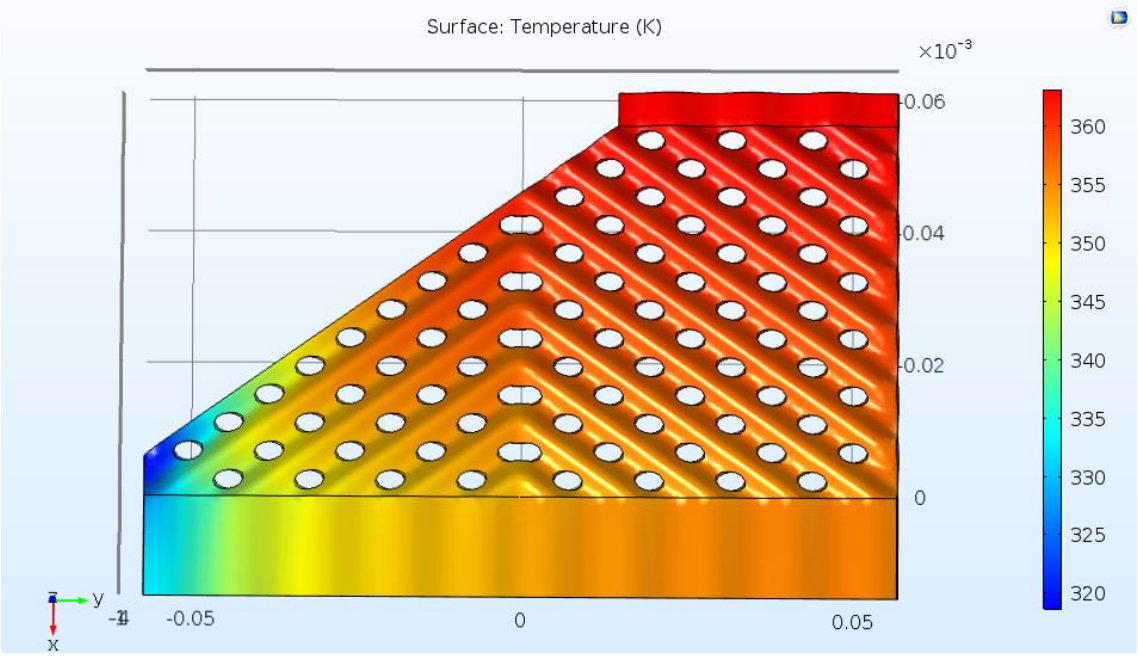

Figure 32. Resulting temperature distribution from a constant heat flux in the full size model for the Reynolds number investigations at inlet velocity 0.5 m/s.

4.3.1 Viscosity

Velocity distribution results from the viscosity investigation in the full-size distribution zone can be seen in Figure 33. The velocity distribution across the outlet is also visible in Figures 34 and 35. The difference is clearest between Shell Rimula 40 and water at $\Delta T=10°C$ according to Figures 33, 34 and 35. Water distributes more uniformly across the outlet, indicated by the lower difference between minimum and maximum graph values and the flatter overall trend. The higher velocities occur closer to the inlet side of the geometry for both fluids, even if it is clearer for oil than water in Figures 34 and 35. However, Shell Rimula 40 has both higher maximum and lower minimum velocity than water. The highest flow velocity is approximately 10 times greater than the lowest indicating a clear flow maldistribution across the outlet. With decreased heat flux, the difference between highest and lowest velocities decreases. These results indicate that flow distribution is dependent of viscosity. The velocity in the middle region of the outlet stays intact despite halving the outward heat flux.

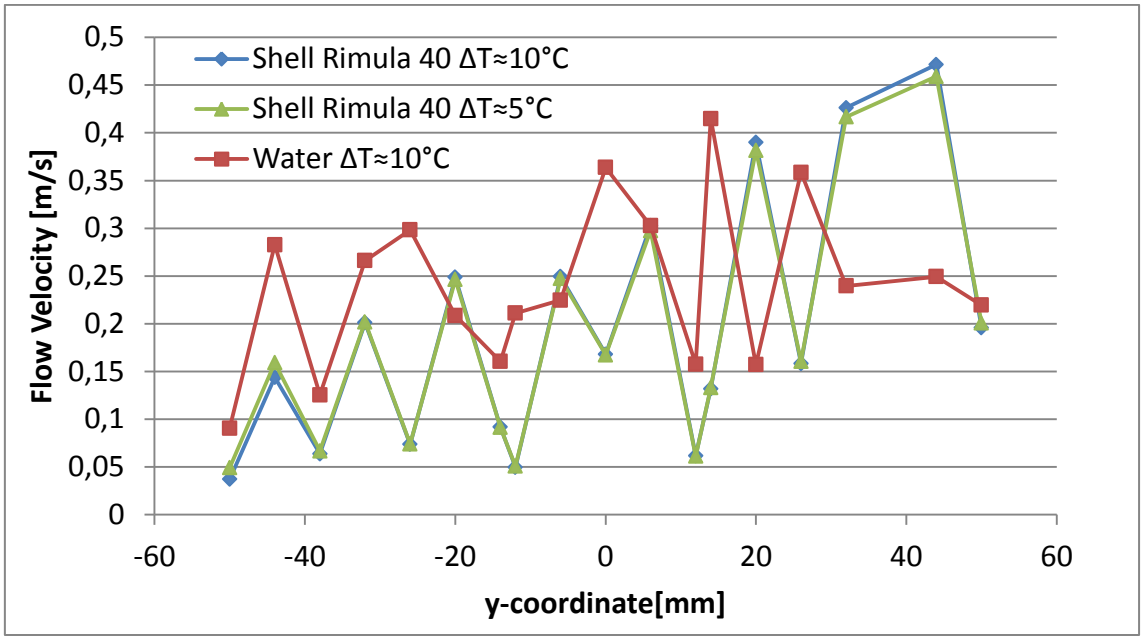

Figure 33. Shell Rimula 40 and water outlet velocity as a function of y-coordinate and different degrees of cooling in the full-size distribution model.

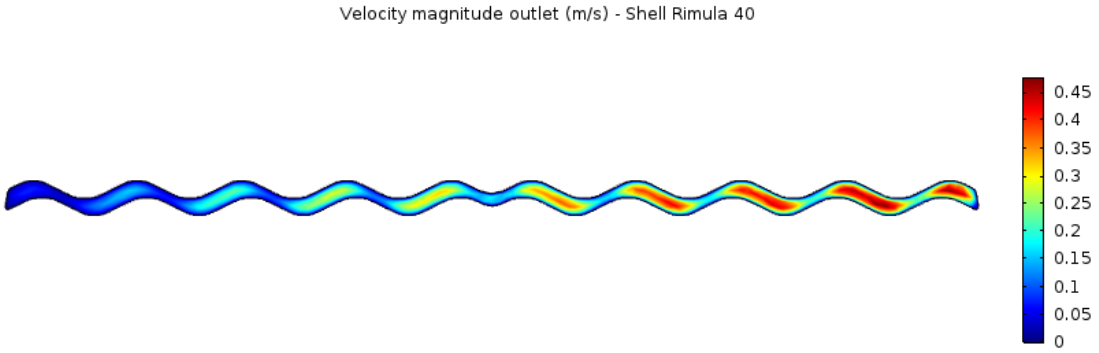

Figure 34. Velocity distribution across the outlet boundary for a 10°C cooling for Shell Rimula 40 and an inlet velocity of 0.5 m/s.

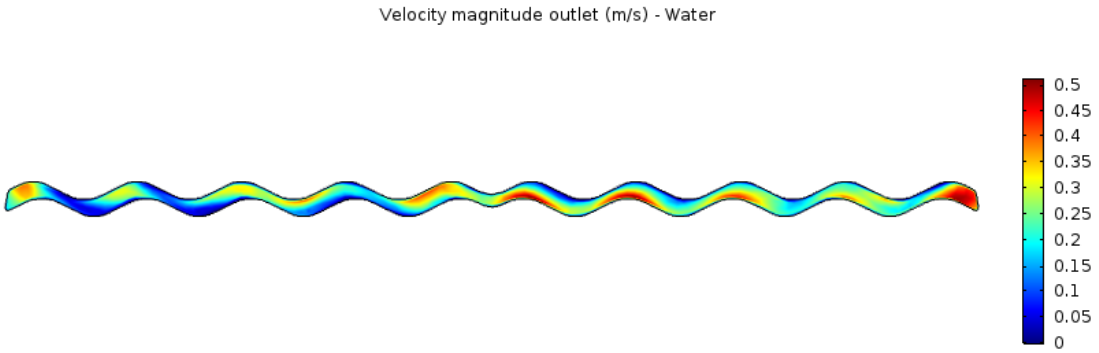

Figure 35. Velocity distribution across the outlet boundary for a 10°C cooling for Water and an inlet velocity 0.5 m/s.

4.3.2 *Gravity*

The outlet velocity distribution from the gravity investigation can be seen in Figure 36. Results show that gravity orientation alone does not affect the flow distribution noticeably. The results without and with gravity in positive and negative x-direction are the same. As in the viscosity case above, higher velocities occur closer to the inlet side of the geometry. The expected behavior from the simplified model results was followed even in the full-size distribution model.

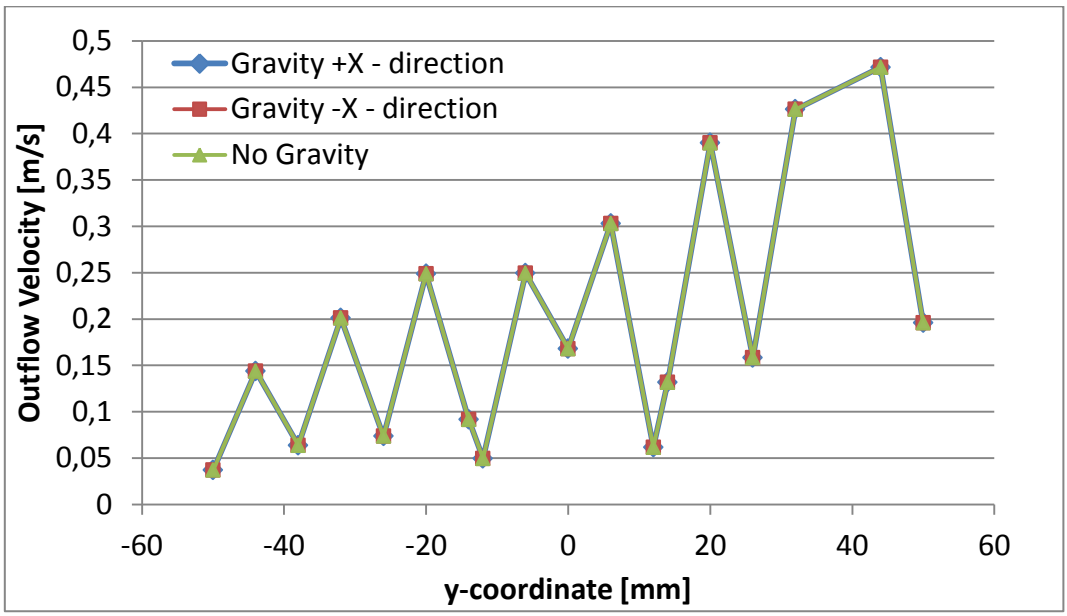

Figure 36. Shell Rimula 40 outlet velocity at different y-coordinates without and with gravity in opposite x-directions.

4.3.3 *Reynolds Number*

Resulting velocity distribution across the outlet for different inlet velocities can be seen in Figure 37. The velocity distribution is also presented in Figures 38 and 39 for inlet velocities 0.5 and 1.5 m/s. The velocity in each point and the overall fluctuations magnitude increases with inlet velocity. Fluctuations in the graph depend on where the measure points are placed since the velocity varies with the varying cross sectional area and the distance to the closest wall (no-slip). Since inlet velocity was varied, it is hard to draw a conclusion about the flow distribution from Figure 37. Another graph was produced and represented flow velocity in each point in percent to the maximum occurring velocity in Figure 40. The maximum velocity occurred at the y-coordinate 0.044 m for all cases and this point was used as reference for the calculations. As the inlet velocity increases in Figure 40, the outlet velocities get larger in comparison to the maximum velocity for the case. This can be seen as the higher lines for higher inlet velocities. In other words, flow is gradually getting more evenly distributed as inlet velocity increases. A high inlet velocity therefore counteracts flow maldistribution, as it was proven in the simplified Reynolds number model.

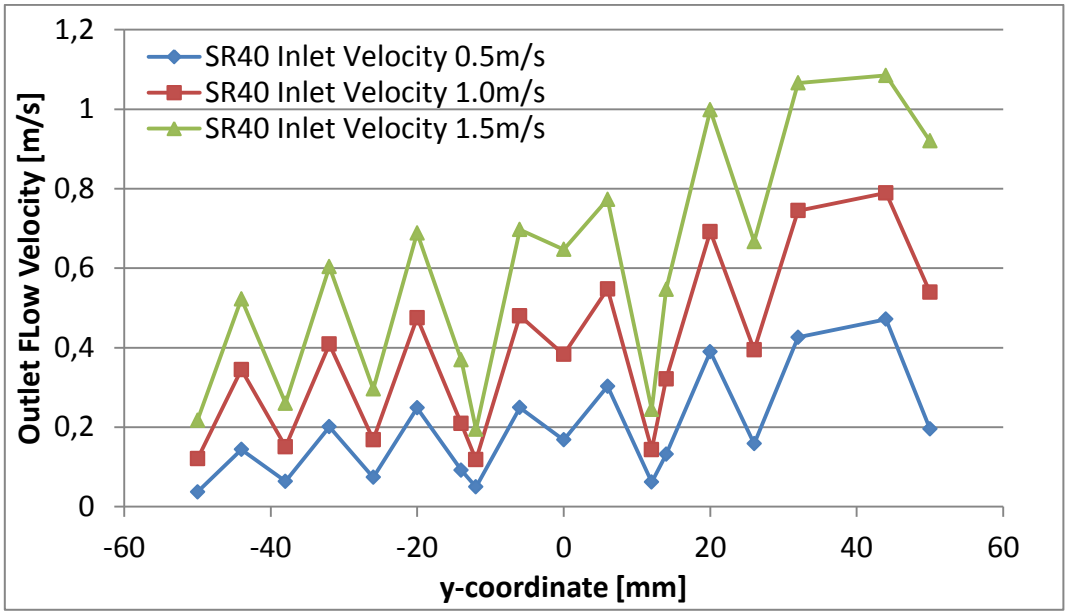

Figure 37. Flow distribution for different Reynolds numbers, presented in flow velocities at different y-coordinates for Shell Rimula 40.

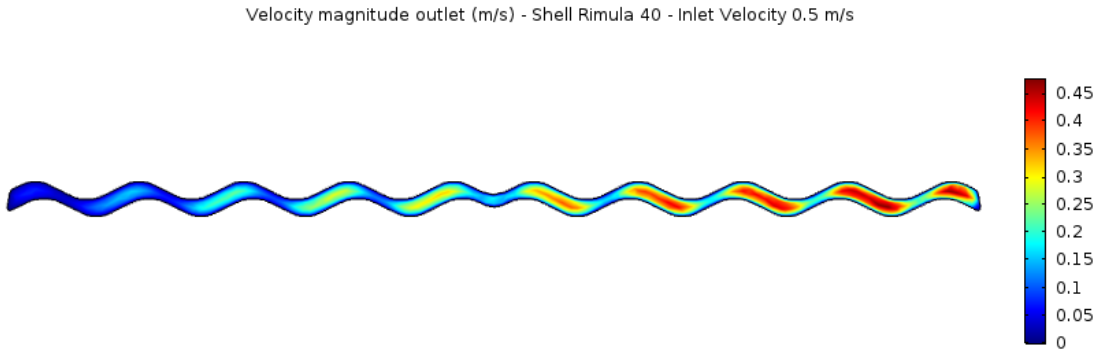

Figure 38. Velocity distribution across the full-size model outlet for Shell Rimula 40 at inlet velocity 0.5 m/s.

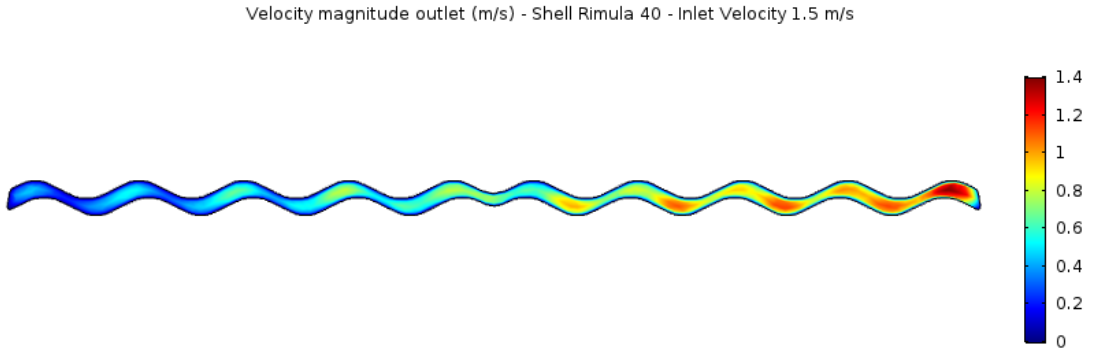

Figure 39. Velocity distribution across the full-size model outlet for Shell Rimula 40 at inlet velocity 1.5 m/s.

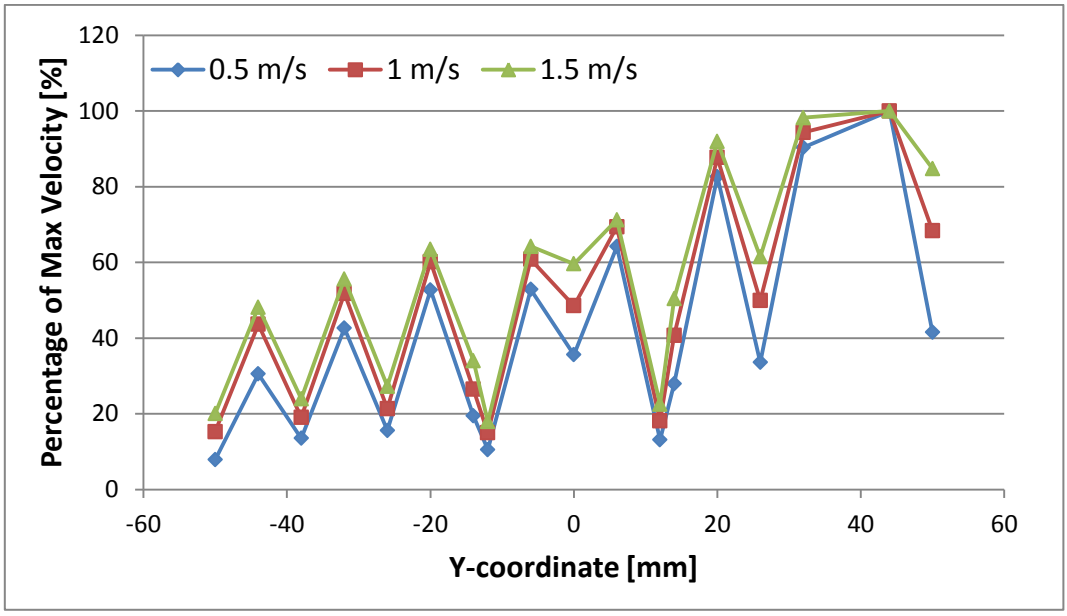

Figure 40. Velocity in each point in percent of maximum velocity in the full size distribution zone model.

5 Discussion

5.1 Validation & Mesh Independence Study

A model that does not reflect reality in some degree is difficult to use, even for smaller and simpler purposes. The models used in this study were validated through comparison with known physical expressions. It would have been optimal to use experimental data from prototypes run under the same operating conditions. The lack of prototypes and experimental data forced the validation process to use available physical correlations. This is particularly true for the simplified models that were created for this study alone. A slight possibility for experimental data validation existed in the full size model. However, a known problem arises when it comes to measuring flow distribution in BPHEs (Sarraf et al. 2015). Since the model only represents a fraction of a brazed plate heat exchanger channel, this gets even more complicated. High performance hardware may lead to a possibility to simulate complete flow channels, which in turn would make it easier to compare results with experimental data. This is a subject for further studies.

Correlations used for validation of the simplified models include uncertainties. Simulations and validation expressions can therefore not be expected to match fully. Validation of the simplified geometries was based on a relationship of pressure drop. This relationship is based on assumptions of constant pipe diameter, fluid properties, velocity and temperature. Despite this limitation, no better suited correlation was described in literature. Even fewer expressions describe fluid behavior in the full-size geometry, which therefore had to be validated through an expected outlet temperature. This method was judged more accurate than the expressions used in the simplified models. With this is mind, it was expected that validation and simulation results would match to a higher degree.

Validation methods should include the parameters investigated with the model in a later stage. In this way, it is possible to control the results with regard to the interesting parameters. Viscosity was included in the validation process of the simplified viscosity model. The model showed an arbitrary agreement with the derived mass flow to viscosity ratio. Gravity was not included in the validation process of the gravity and Reynolds model. Instead the length difference between the channels was used. It was hard to validate the model with respect to both Reynolds number and gravity at the same time. Velocity was included for validation but gravity was not. The agreement among pressure, length and velocity, was good, and the model was considered validated. Based on this, there is no reason to think that a validation including gravity would give another result.

In the validation of the viscosity model, a spike can be seen in the graphs close to the inlet of the hot channel. This peak is clearer for the hot channel and initiates a relatively large difference between ratios that fades further away from channel inlet. The temperature in this region is unchanged while an increase in velocity is noticeable, as can be seen in Figures 21 to 23. Higher values in Figure 15 are therefore expected at the beginning of the hot channel. Validation mainly focused on the fluid behavior after this region and before the rejoining region. As the temperature and velocity profiles develop along the channel length, differences between lines decreases. Based on this behavior, the model was considered validated.

The gravity and Reynolds number model was validated with pressure drop correlations. Figure 17 shows an increasing difference between ratios as the angle is increased. This could be explained with an introduction of minor losses that increases with angle (Cengel & Cimbala 2010). The change in flow direction, due to the elbow, leads to a loss beyond the overall flow loss. Since the loss increases with angle, a difference is expected to develop and increase with angle. With this and the relatively small differences in mind, the model was considered validated

The full size model was validated through an expected temperature difference from a calculated and defined constant heat flux. As temperature and flow behavior are strongly linked through temperature dependent fluid properties, a validation of one indicates validation of the other. This is especially useful for this geometry where flow is hard to validate. An expected cooling of 10 °C would not be achieved if the flow behavior differed from what is expected from general physics. A slightly higher temperature difference than expected was observed with a *surface average* in COMSOL. This is mainly because of the difference in flow lengths to the different points of the outlet together with the constant heat flux. If the few points with much lower temperatures were excluded from the average temperature, the temperature difference would have been closer to the expected. As the 10°C difference was valid at a large portion of the outlet, and the physical behavior was followed by the deviant points, the model validation was considered sufficient.

The choice of mesh in the respective models was based on the results of the mesh independence study as well as number of elements and computational time. For the simplified models, this resulted in mesh qualities that may not be optimal for absolute values but enough for studying trends and differences. Increased mesh qualities gave small differences in results, according to Figures 15, 16, 17 and 18, but in some cases unreasonable computational requirements. The mesh of the full-size model was more important but even harder due to the high detail level geometry. In this case, it was impossible to use mesh at finer qualities than normal due to the lack of computer memory. The simulations at normal mesh quality ran at the edge of computer memory throughout. However, only a small increase in simulation accuracy could be observed in Figures 19 and 20 between coarse and normal which indicates that the change is even smaller between normal and fine. The meshes used were considered good enough.

The mesh independence study showed a decrease in number of elements with increased angle for the gravity and Reynolds number model. The reason to this is not obvious since a longer channel should give more elements. The explanation could be found in the automatic mesh tool's handling of sharp edges. As the sharpness of the dividing edge is increased, COMSOL could see this as a reason to higher detail level in that particular area. With this explanation, a lower angle would yield a higher number of elements.

5.2 Method

The full size model outlet section velocities were investigated rather than the mass flow through different sections. This was mainly due to difficulties in dividing the outlet boundary into sections in COMSOL. Importing geometries from other software can be an easier approach but can also mean complications like this. COMSOL could not fully handle the approximated surfaces of the imported geometry. Tries to divide the outlet surface into sections failed and therefore velocity in certain points was investigated instead.

Parameters investigated were three out of a total of six. The choice of these parameters was based on theory and a meeting with SWEP. The parameters in the outlet velocity expression (6) that are not investigated, can however be related to the chosen parameters. Height effects are indirectly included in the gravity results in this study. Height difference was shown as the main reason to the gravity effects. The flow length and hydraulic diameter are both decisive for pressure drop and therefore also flow velocity. The effect of these two is therefore indirectly included in the Reynolds number investigations.

5.3 Results

The viscosity results in the simplified model were expected. A higher temperature leads to lower viscosity and therefore higher mass flow. The effect was noticeable even at lower temperature differences between the hot and cold channels. As viscosity of oil is more temperature dependent than water, a temperature difference creates a higher flow maldistribution. This was visible in both the simplified and the full-size model. Change in flow distribution between 10 and 5°C differences was small. This is explained with the small viscosity changes with temperature at the respective temperature range for Shell Rimula 40. If lower temperatures would have been analyzed with the same temperature differences between the hot and cold channels, the viscosity impact would have been greater. Oil cooling applications are kept in mind in these investigations which normally occur at temperatures around 80 – 100 °C as investigated. The results show that it is important to consider the fluids used and the temperature range involved in a plate heat exchanger. Differences in fluid properties and operating conditions make it important to consider viscosity impact in each individual case. The flow distribution is dependent on the fluid and the temperatures involved. Due to differences in fluid properties and operating conditions, the impact of viscosity differences will have to be considered in each individual case. These results point towards that maldistribution not necessarily occur as a result of the fluid viscosity itself, but as a result of the viscosity temperature dependency.

There was no effect of varying gravity between the flow direction and opposite the flow direction. A slightly higher flow velocity was observed in the straight channel, explained by the shorter channel and therefore less flow losses. With gravity in the flow direction, the flow gains pressure as it converts potential pressure to kinetic pressure. When gravity is oriented in the opposite direction, kinetic pressure is instead converted to potential. As long as the pressure drop difference between fluid paths is the same, the flow distributes in the same way. This was not clear before the study but explains the results. The only situation where gravity has an effect on flow distribution is when a height difference between fluid paths is introduced. Since height travelled for all paths is the same when gravity acts along or opposite the flow direction, the flow distribution should be the same in the two cases. This was also checked by the introduction of gravity in the direction normal to fluid flow in the simplified model. A strong dependency of gravity was then observed. This was not possible in the full-size model due to convergence problems explained by the large velocity gradients seen in the simplified model. Since the other simplified investigations were followed by the full-size model, there is no reason to think that the gravity results from the full-size model would deviate from the simplified ones.

Results from simplified cases show that gravity does not affect flow distribution if a plate heat exchanger is placed vertically, which is the most common orientation. However, in the few situations where main flow occurs horizontally; care must be taken to avoid flow maldistribution. This is especially true if the inlet and outlet ports are placed on the same side of the fluid channel. A difference in height between paths would then introduce a

higher flow in parts at lower height relatively to the ports. It should be kept in mind that gravity affects the overall pressure drop in the system. A high viscous fluid could be allowed to flow in the same direction as gravity to minimize the required pumping power.

A variation of Reynolds number had an effect on flow distribution. In the simplified model, this can be seen in Figures 28 and 29. It can also be seen in the full-size model in Figures 37 and 40. Both models point towards the same results. Higher Reynolds number creates a more even flow distribution at the outlet. The effect in percentage points of increased velocity is approximately the same regardless of fluid. This is true even if Shell Rimula 40 has a higher degree of maldistribution at the start. One explanation to the more even flow distribution at higher velocities can be found in the length difference. As the velocity is increased, the impact of length difference to the overall pressure loss decreases. This means that the total pressure loss difference between the channels decreases with increasing velocities.

It seems that a high Reynolds number has a small but positive effect on flow distribution. This means that it is favorable to strive for higher channel velocities from a flow distribution point of view. High velocities are typically unwanted in channel flow since pressure drop increases exponentially with velocity. This can be seen from the second term in the pressure form of the Bernoulli equation (1) where the kinetic pressure drop increases exponentially with flow velocity. Too low as well as too high velocities should therefore be avoided in plate heat exchangers for optimal flow distribution.

5.4 Study

It was known before this study that CFD modeling of plate heat exchangers require high performance computers. This was also the reason behind the lack of studies in the area. Although this study was made with hardware that is below what is considered enough by the industry, the simulation results were judged adequate for basic conclusions. Resulting values in this study should not be interpreted as absolute, but rather serve as guidelines for further studied and theories.

6 Conclusion

Many advantages of brazed plate heat exchangers could make them suitable for oil cooling applications. A problem arises with highly viscous fluids like oil since high viscosities can lead to flow maldistribution within the BPHE. To fully use the potential of BPHEs, it is important that fluids distribute evenly over the available heat transfer surfaces. Flow distribution is difficult to measure if the plate heat exchanger is welded or brazed together. This is a case where much work can be saved by the use of CFD. This study was made to investigate parameters that may affect flow distribution inside brazed plate heat exchangers. Velocity, viscosity and gravity were chosen for this study and their respective effects were investigated in COMSOL Multiphysics.

It was shown that viscosity has an effect on flow distribution in plate heat exchangers. The magnitude of the effect is dependent of the temperature dependency of the fluid viscosity. Since viscosity and its temperature dependency vary with fluid, it is important to consider possible effects for each fluid and respective operative condition.

Gravity has a negligible effect on flow distribution in vertical placement of the plate package. As gravity acts in the direction perpendicular to flow it has major effect on flow distribution. It is therefore important to consider gravity effects in horizontally placed plate packages. Especially if the inlet and outlet ports are placed on the same side of the plate package and induce a height difference between flow paths.

High Reynolds numbers have positive effects on flow distribution. An increase in flow rates can even flow distribution over the heat transfer area. However, high flow rates mean high flow losses and should be avoided. This means that the lowest flow velocities should be avoided to even flow distribution and the highest should be avoided to minimize flow losses.

7 Future Studies

There are many parameters beyond those analyzed in this report that is responsible for flow distribution. Geometrical parameters such as chevron pitch, height and angle are as well as fluid properties responsible for flow distribution inside plate heat exchangers. Further studies could involve developing distribution zone patterns that optimizes flow distribution with respect to fluid properties and working conditions. For this to be possible, further studies about other and the same fluid properties as in this study are also needed to map fluid behavior inside plate heat exchangers. The constant increase of available computational hardware makes it possible to enlarge this study to larger fluid sections and, in time, complete plate packages.

8 References

Aslam Bhutta, M.M., Hayat, N., Bashir, M.H., Khan, A.R., Ahmad, K.N. & Khan, S. (2012). CFD applications in various heat exchangers design: A review. *Applied Thermal Engineering,* 32 , 1-12.

Autodesk Inc. (2015). *Finite Element vs Finite Volume.* [Online] Available from: https://knowledge.autodesk.com/support/cfd/learn-explore/caas/CloudHelp/cloudhelp/2014/ENU/SimCFD/files/GUID-12A9AED8-2047-4D3A-BC80-82BE9CF47517-htm.html [2016-4/5].

Baode Heat Exchanger Co. (2009). *Baode Gasket Plate Heat Exchanger Features.* [Online] Available from: http://www.bd-heatech.com/Gasket_Plate_heat_exchanger_features.htm [2016-05/24].

Bonnett, A.H. (2001). Operating Temperature Considerations and Performance Characteristics for IEEE 841 Motors. *IEEE Transactions on Industry Applications,* 37 (4), 1120.

Cengel, Y. & Cimbala, J. (2010). *Fluid Mechanics - Fundamentals and Applications.* (2nd edn.). New York: McGraw-Hill.

CFD Online. (2011). *Finite Element.* [Online] Available from: http://www.cfd-online.com/Wiki/Finite_element [2016-4/6].

CFD Online. (2012). *Finite Volume.* [Online] Available from: http://www.cfd-online.com/Wiki/Finite_volume [2016-4/6].

COMSOL AB (2015). *COMSOL Multiphysics Documentation.* (5.2nd edn.). COMSOL AB.

COMSOL Inc. (2016a). *COMSOL Multiphysics.* [Online] Available from: https://www.comsol.com/comsol-multiphysics [2016-4/5].

COMSOL Inc. (2016b). *Finite Element Mesh Refinement.* [Online] Available from: https://www.comsol.com/multiphysics/mesh-refinement [2016-04/20].

COMSOL Inc. (2016c). *The Finite Element Method (FEM).* [Online] Available from: https://www.comsol.com/multiphysics/finite-element-method [2016-4/5].

Davin, T., Pellé, J., Harmand, S. & Yu, R. (2015). Experimental study of oil cooling systems for electric motors. *Applied Thermal Engineering,* 75 , 1-13.

Dović, D., Palm, B. & Švaić, S. (2009). Generalized correlations for predicting heat transfer and pressure drop in plate heat exchanger channels of arbitrary geometry. *International Journal of Heat and Mass Transfer,* 52 , 4553-4563.

Freund, S. & Kabelac, S. (2010). Investigation of local heat transfer coefficients in plate heat exchangers with temperature oscillation IR thermography and CFD. *International Journal of Heat and Mass Transfer,* 53 , 3764-3781.

Galeazzo, F.C.C., Miura, R.Y., Gut, J.A.W. & Tadini, C.C. (2006). Experimental and numerical heat transfer in a plate heat exchanger. *Chemical Engineering Science,* 61 , 7133-7138.

Gerenmark, P. (2016). *Plate Heat Exchangers.* Landskrona: SWEP.

Gullapalli, V.S. (2011). Design of High Efficiency Compact Brazed Plate Heat Exchangers using CFD. In *IIR International Congress of Refrigeration.* Prague, Czech Republic: .

Gullapalli, V.S. & Sundén, B. (2011). Generalized performance analysis of compact brazed plate heat exchangers. In *21st national and 10th ISHMT-ASME heat and mass transfer conference.* Madras, India: .

Gullapalli, V.S. & Sundén, B. (2014). CFD Simulation of Heat Transfer and Pressure Drop in Compact Brazed Plate Heat Exchangers. *Heat Transfer Engineering,* 35 (4), 358-366.

Han, X., Cui, L., Chen, S., Chen, G. & Wang, Q. (2010). A numerical and experimental study of chevron, corrugated-plate heat exchangers. *International Communications in Heat and Mass Transfer,* 37 , 1008-1014.

Jeong, J.Y., Hong, H.k., Kim, S.K. & Kang, Y.T. (2009). Impact of plate design on the performance of welded type plate heat exchangers for sorption cycles. *International Journal of Refrigeration,* 32 , 705-711.

Lee, J. & Lee, K. (2014). Flow characteristics and thermal performance in chevron type plate heat exchangers. *International Journal of Heat and Mass Transfer,* 78 , 699-706.

Lee, J. & Lee, K. (2015). Research paper: Friction and Colburn factor correlations and shape optimization of chevron-type plate heat exchangers. *Applied Thermal Engineering,* 89 , 62-69.

Logan, D.L. (2007). *A First Course in the Finite Element Method.* (4th edn.). Toronto Canada: Nelson.

Rangaprasad, R.R. & Gupta, A. (2015). Recent trends in packaging of industrial/automotive lubricants. *Popular Plastics & Packaging,* 60 (2), 57-60.

Sarraf, K., Launay, S. & Tadrist, L. (2015). Complex 3D-flow analysis and corrugation angle effect in plate heat exchangers. *International Journal of Thermal Sciences,* 94 , 126-138.

Shah, R. & Sekulic, D. (2003). *Fundamentals of Heat Exchanger Design.* (1st edn.). Hoboken, New Jersey: John Wiley & Sons Inc.

SWEP International AB. (2015a). *About SWEP*. [Online] Available from: http://swep.net/company/company/ [2016-5/23].

SWEP International AB. (2015b). *B10*. [Online] Available from: http://www.swep.se/products/b10/ [2016-05/18].

SWEP International AB (2015). *SSP G7*. http://www.swep.net/support/ssp-calculation-software/ssp-g7/: SWEP International AB.

Tsai, Y., Liu, F. & Shen, P. (2009). Investigations of the pressure drop and flow distribution in a chevron-type plate heat exchanger. *International Communications in Heat and Mass Transfer,* 36 (6), 574-578.

Versteeg, H.K. & Malalasekera, W. (2007). *An Introduction to Computational Fluid Dynamics - The Finite Volume Method*. (2nd edn.). Harlow England: Pearson Education Limited.

Wang, T., Gu, B., Zhao, P. & Qian, C. (2015). Numerical investigation of liquid cooling cold plate for power control unit in fuel cell vehicle. *Microelectronics Reliability,* 55 (7), 1077-1088.